

# The spectrometric practical voltage: determination of X-ray tube voltage up to 300 kV by in-beam X-ray spectrometry with a cadmium telluride detector

Jaroslav Šolc<sup>1</sup>,<sup>a,\*</sup> Stefan Pojtinger<sup>2</sup>,<sup>b</sup> Jana Šmoldasová<sup>1</sup>,<sup>a</sup> Vladimír Sochor<sup>1</sup>,<sup>a</sup> and Jan Rusňák<sup>1</sup>,<sup>a</sup>

<sup>a</sup>Czech Metrology Institute (CMI), Okružní 31, CZ-638 00 Brno, Czech Republic

<sup>b</sup>Physikalisch-Technische Bundesanstalt (PTB), Bundesallee 100, D-38116 Braunschweig, Germany

E-mail: [jaroslav.solc@cmi.gov.cz](mailto:jaroslav.solc@cmi.gov.cz)

**ABSTRACT.** This paper describes a method for determining the energy of the X-ray spectrum end-point ( $E_{\text{end}}$ ) by means of X-ray spectrometry performed with a CdTe detector. Designated the spectrometric practical end-point (SPE) method, this technique is based on the comparison of the high-energy part of the measured detector spectrum with a detector spectrum obtained using Monte Carlo calculations. It combines findings and results from a detector characterization previously done for the purpose of unfolding the X-ray fluence spectra. Here, the influences of tube current, tube voltage ripple, detector count rate, and the choice of calibration radionuclide sources were studied. The findings for the latter two parameters led to the modification of a procedure for energy calibration of the detector as well as to updated parameters of the charge carrier transport (CCT) and Gaussian energy broadening (GEB) models valid for high-count-rate measurements. Additionally, the influence of improper energy calibration and of neglecting the CCT and GEB effects on the main characteristics of the unfolded X-ray fluence spectra was analyzed to provide an overview of systematic errors. A quantity obtained with the SPE method, the spectrometric practical voltage (SPV), is introduced. It is demonstrated that the SPV agrees with the practical peak voltage within 0.03% when the voltage ripple of a high-voltage generator is below 2%. A comparison done at PTB, Germany, of the SPV to voltage divider readings showed relative and absolute differences between the reading and the SPV of between 0.1% and 0.8% (0.15 keV to 1.16 keV) in the 20 to 300 kV tube voltage range. Its combined uncertainty varied between 0.13 and 0.33 keV for continuous beam N-series qualities ranging from 10 to 300 kV. The SPE method was then used to determine  $E_{\text{end}}$  of N-series qualities realized at Czech Metrology Institute. Also, the difference between  $E_{\text{end}}$  as obtained with the SPE method and that found with a simple linear fit of the straight high-energy part of the detector spectra was evaluated, revealing a difference of between  $-0.2$  and  $+1.5$  keV for N-series qualities up to 300 kV. The SPE method is suitable for users who have already implemented an in-beam X-ray spectrometry technique and seek to determine the tube voltage but do not possess a voltage divider.

**KEYWORDS:** Spectrometers; Gamma detectors (scintillators, CZT, HPGe, HgI etc); X-ray detectors; Solid state detectors

\*Corresponding author.

---

## Contents

<b>1</b>	<b>Introduction</b>	<b>1</b>
<b>2</b>	<b>Materials and methods</b>	<b>3</b>
2.1	The detector	3
2.2	Measurement setup	3
2.3	Radionuclide sources	4
2.4	Radiation qualities	4
2.5	X-ray sources	4
2.6	Voltage dividers at PTB	4
2.7	Quantities describing voltage	5
2.8	Spectrometric practical voltage	6
2.9	Preparation work	7
2.10	End-point energy	8
2.11	Influence of the tube current	12
<b>3</b>	<b>Results and discussion</b>	<b>12</b>
3.1	Additional characterization of the detector	12
3.2	End-point energy	19
3.3	Influence of voltage ripple	23
3.4	Comparison of quantities	25
3.5	Influence of the tube current	26
<b>4</b>	<b>Conclusions</b>	<b>27</b>
<b>5</b>	<b>Abbreviations</b>	<b>28</b>
<b>A</b>	<b>Systematic errors caused by omission of detector effects</b>	<b>30</b>

---

## 1 Introduction

In 2018, Czech Metrology Institute (CMI) adopted the method of in-beam X-ray spectrometry up to ~300 kV using a compact CdTe detector. Continuous characterization of the detector [1], improvement of the measurement geometry [2], and an optimized method for unfolding the energy distribution of primary photons [3] created a set of tools that allowed the spectrometric determination of the end-point energy ( $E_{\text{end}}$ ) of X-ray fluence spectra.

The X-ray tube voltage is one of the main parameters defining the X-ray fluence spectrum. As CMI is the national metrology laboratory, its main concern in determining the tube voltage is to fulfill the requirements for reference or characterized spectra used in the calibration or verification of instruments, e.g., [4, 5, 21]. Elsewhere, for example in the field of diagnostic radiology, the primary reason for knowing the tube voltage is the fact that slight changes in this voltage can lead

to significant changes in the absorbed dose in routine diagnostic procedures [6–8] or degrade the image contrast [10]. Routine monitoring of the tube voltage was also suggested by the American Association of Physicists in Medicine (AAPM) [11].

The tube voltage can be determined by invasive or non-invasive methods. Invasive methods use a suitable meter or a high-voltage divider connected directly to the high-voltage generator of the X-ray tube. The non-invasive methods primarily include kVp meters [12] or X-ray spectrometry utilizing direct, Compton recoil, or X-ray fluorescence measurement methods coupled mainly with silicon photodiodes or high-purity germanium (HPGe), silicon, CZT, or CdTe detectors. More detailed information about these methods can be found elsewhere ([7–9, 13]).

Currently, all international standards for reference radiation conditions recommend the use of high-voltage dividers instead of spectrometry-based approaches because it is assumed that the required measurement uncertainty cannot be achieved using non-invasive methods. The current version of ISO 4037-1 [21], which defines conditions for the characterization and production of reference photon fields intended for the calibration of protection-level dosimeters, states that “the measurement of the maximum photon energy by high-resolution spectrometry is not recommended.” The current version of the IEC 61267:2005 [5] standard on the establishment of reference radiation conditions for the determination of characteristics of medical diagnostic X-ray equipment generally does not allow the use of non-invasive methods. However, since the purchase and periodic calibration of a voltage divider are much more expensive than for an X-ray spectrometer [8, 14], spectrometry is an attractive alternative.

The increasing interest in and knowledge of X-ray spectrometry in the ionizing radiation metrology community combined with the availability of compact spectrometers might lead to efforts to reinstate spectrometry alongside voltage dividers as an accepted method for measuring tube potential [8, 14]. As CMI does not possess a voltage divider and does not foresee obtaining one, such an initiative would align with current practicalities at CMI.

Before the purchase of a CdTe spectrometer,  $E_{\text{end}}$  had only been measured once at CMI back in the early 2000s. An HPGe detector with liquid nitrogen cooling was used and  $E_{\text{end}}$  was obtained from an intersection of a linear fit of the detector spectrum end part and a linear fit of background, as described by other authors [8, 14, 15, 33]. The measurement setup was complicated and time consuming and the measurements were not repeated. When a compact, electrically-cooled CdTe detector became available on the market and was later purchased by CMI,  $E_{\text{end}}$  was estimated from the measured spectra as an ancillary result of a procedure for unfolding the primary X-ray fluence spectrum [3]. Two methods were used: the first method calculated the minimum of  $E_0 - E(y = 0)$ , where  $E(y = 0)$  is the energy where a tangent line at energy bin  $E_0$  of the spectrum reached  $y = 0$ . The second method utilized the linear fit mentioned above. It was stated that the accuracy is sufficient for the determination of the maximum energy of the response matrix needed for the unfolding of the given fluence spectrum but that a different method might be needed for the purpose of determining the exact tube voltage [3]. Such a method is described in the present paper. This method is intended for use in a calibration laboratory, but can be adapted for in-field measurements as well. The goal of this work is to introduce a clear methodology for determining tube voltage by X-ray spectrometry that might also be useful as a basis for discussing the possible re-introduction into the relevant international standards of spectrometry-based tube voltage measurements, which had previously been permitted, e.g., by the now obsolete ISO 4037:1996 [16].

## 2 Materials and methods

### 2.1 The detector

X-ray beam spectrometry was performed using a compact commercial detector, the X-123CdTe (AMPTEK, Inc., U.S.A.) [17], with a sensitive element made of cadmium telluride (CdTe) compound and the entrance window made of 100  $\mu\text{m}$  thick beryllium alloy. The detector was connected to the measuring computer directly via a USB active repeater cable. The detector setup and spectra acquisition were performed in the DppMCA software [18] provided by the detector manufacturer. More information about the detector can be found elsewhere [1, 17]. The detector settings remained the same as described in [1]. In summary, the detector cooling temperature was 220 K, high-voltage bias +950 V, peaking time 2.4  $\mu\text{s}$ , flat top width 0.6  $\mu\text{s}$ , fast threshold 9.93, fast peaking time 100, the advanced base time restoration mode was 1, the pile-up rejection setting was turned on, and the rise time discrimination was turned off. Dead time and live time were determined by the DppMCA software. The total count rate was calculated as the sum of counts in all channels in the acquired spectrum divided by the live time.

### 2.2 Measurement setup

The measurement setup consisted of a camera rail slider with two independent platforms attached and horizontally movable transverse to the beam axis (figure 1). One movable platform held the alignment platform with the collimator and the other one held the detector. The collimator consisted of the front tungsten shielding, the steel body, and the outer side and rear shielding made of a combination of lead and tungsten encapsulated in a cover printed on a 3D printer from plastics containing homogeneously distributed steel [19] and tungsten [20] powder. After the collimator axis had been aligned towards the tube focus point [2], the detector was inserted into the collimator. Three collimation disks, each made of 2 mm thick tungsten, were selected from the set consisting of disks with nominal aperture diameters of 100  $\mu\text{m}$ , 200  $\mu\text{m}$ , 400  $\mu\text{m}$ , 1 mm, and 2 mm and inserted into the collimator to control the photon flux at the sensor. Spectra generated with a tube voltage > 150 kV were acquired with an additional collimator made of 29 mm thick lead and positioned before the front tungsten shielding. See [2] for more details.

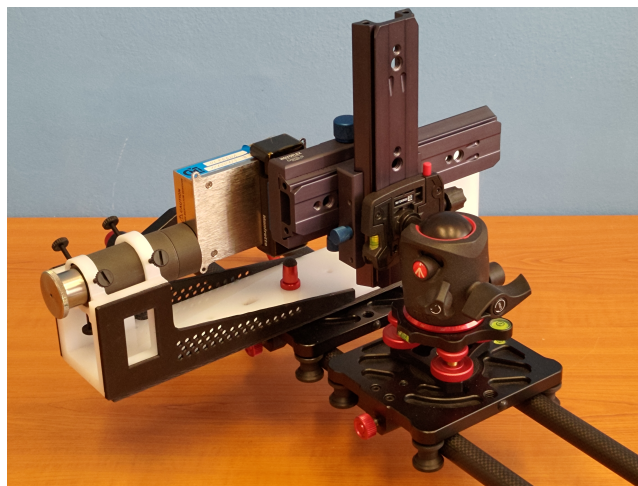


**Figure 1.** Setup for the measurement of X-ray spectra with an X-123CdTe spectrometer.

### 2.3 Radionuclide sources

Sealed point-like ( $\sim 3$  mm diameter and  $\sim 0.2$  mm height)  $^{241}\text{Am}$  and  $^{133}\text{Ba}$  radionuclide sources centered in a total of 3 mm thick polystyrene encapsulation and small sealed  $^{57}\text{Co}$  and  $^{152}\text{Eu}$  sources encapsulated in a steel cover were used in this study for detector response characterization. The point-like sources were produced by CMI and they were traceable to the Czech national standard for the activity of radionuclides.

### 2.4 Radiation qualities

$E_{\text{end}}$  was determined using narrow series (N-series) X-ray qualities realized at the national metrological laboratories of the Czech Republic (CMI; Czech Metrology Institute located in Prague) and Germany (PTB; Physikalisch-Technische Bundesanstalt located in Braunschweig). The N-series qualities are the reference radiation qualities for calibrating protection-level dosimeters and doserate meters in operational quantities [21].

Some effects discussed in this study are also demonstrated on the RQR-series [5] and the TW-series radiation qualities [22]. Both series consist of wide spectra due to low additional filtration. The RQR qualities simulate most entrance beams used in diagnostic radiology and they are applied in determining the characteristics of medical diagnostic X-ray equipment. The TW qualities are used for the dose-to-water calibration of equipment employed for measurement in X-ray therapy beams. The RQR and TW qualities realized at CMI are generated with a nominal tube voltage ranging from 40 to 150 kV and 10 to 100 kV, respectively.

### 2.5 X-ray sources

At CMI, the radiation qualities up to 150 kV were realized with the 160 kV single-pole generator ISOVOLT 160 HS (Rich.Seifert & KG, Germany) and an MB 161/4 X-ray tube of 3.0 kW maximum power and an inherent filtration of 1 mm beryllium. The voltage ripple was 6 V/mA at 40 kHz according to the manufacturer data sheet. The qualities above 150 kV were realized with the 320 kV double-pole generator PANTAK PMC (Pantak/Seifert, United Kingdom) with an MB 350/1 X-ray tube (THALES, France) of 4.2 kW maximum power and an inherent filtration of 7 mm beryllium. The voltage ripple was  $< 20$  V/mA at 12 kHz according to the manufacturer data sheet. Both systems consisted of a tungsten anode with the target angle of  $21^\circ$  and included a setup for added filtration and a PTW 786 transmission monitor chamber (PTW, Germany).

At PTB, the N-series radiation qualities were realized with the 450 kV generator MGG47 (Yxlon International GmbH, Germany, S/N A30140800031) and an MB450-1H450 X-ray tube (Thales Electron Devices GmbH, Germany, S/N 130174) with 4.5 kW maximum power, an inherent filtration of 7 mm beryllium and a tungsten target. The double-pole system had a ripple of 10 V/mA as specified by the manufacturer. A transmission monitor chamber built by PTB was used to monitor the beam output during the measurement.

### 2.6 Voltage dividers at PTB

The voltage dividers used at PTB and designated 863177N and 863175N are prototypes built at PTB. They reduce the voltage by a factor of 20 000 and have a buffer amplifier to avoid any influence of the connected device used to measure the output. Also, the voltage dividers are frequency compensated

(RC circuits). Above 20 kV, the uncertainty of the division is 0.1% ( $k = 2$ ). Calibration of the voltage divider is performed every ten years.

For measurements, each of the voltage dividers was connected to one pole of the two-pole generator MGG47. Voltage divider 863177N was used for the positive voltages and 863175N for the negative voltages. A digital multimeter, Keithley 2000 (Tektronix Inc., U.S.A.), was connected to the voltage dividers for the measurements of the X-ray generator voltage. The multimeter in direct current (DC) mode was used to determine the mean electric potential at the output of the voltage divider (also referred to below as the “reading”) with an uncertainty of 0.01% ( $k = 2$ ).

For the setup under investigation (MGG47 high-voltage generator and MB450-1H450 X-ray tube), there was no protective resistor between the X-ray tube (e.g., built into the protective tube housing) and the high-voltage output of the generator. Therefore, it was not necessary to apply any correction for an additional voltage drop to the measurements performed with the high-voltage dividers. This is the typical case for most modern generators with high-frequency switching supplies, where protective resistors can be moved into the generator in front of the high-voltage output [21].

## 2.7 Quantities describing voltage

The tube voltage, sometimes also referred to as the tube potential [21], is the potential difference between the cathode and anode of the X-ray tube and defines the energy of accelerated electrons hitting the anode.

The voltage ripple is a percentage difference of the highest and lowest voltage in the time interval relative to the highest voltage [4]. It expresses fluctuations in the voltage output of an X-ray generator.

The (maximum) peak voltage, kVp, also called peak kilovoltage or kilovoltage peak, represents the maximum tube potential accelerating the electrons hitting the target material. It also describes the maximum energy that can be transferred to the X-ray photons by bremsstrahlung and therefore represents the upper energy limit of the corresponding X-ray fluence spectrum. This definition is applied in the present paper, although some detector manufacturers differentiate the kVp into the mean kVp ( $kVp_{\text{mean}}$ , average of all maximum voltages during exposure) and the maximum kVp ( $kVp_{\text{max}}$ ).

In 1998, PTB introduced the practical peak voltage, PPV, of diagnostic X-ray generators [23]. The purpose of this quantity was to characterize an arbitrary waveform of an X-ray generator based on the comparison of the contrast obtained with this generator to the contrast produced by the same X-ray tube connected to a constant potential generator. The PPV is the X-ray tube voltage realized with an ideal constant potential generator that would result in the same ratio of air kerma behind a phantom (10 cm thick polymethyl methacrylate) and air kerma behind the same phantom plus a contrast material (1 mm thick aluminum) as an exposure made with the same X-ray tube connected to the given generator delivering non-constant potential in time [4, 23]. A histogram of voltages influenced by the waveform from the high-voltage generator during the irradiation time must be known in order to calculate the PPV.

Currently, the PPV is the basis for the IEC reference radiation conditions [5]. These reference radiation conditions are in turn referenced by other IEC standards that specify the operation of X-ray equipment [4], and they are commonly used in calibrating diagnostic dosimeters, in the conformity assessment of diagnostic dosimeters, and for comparisons between primary and secondary standard laboratories worldwide.

The PPV approaches the kVp and the mean electric potential on the tube when the voltage ripple of the X-ray generator decreases. This is the case for most modern commercial high-frequency X-ray

generators as they are able to produce nearly constant generating potential with a voltage ripple of less than 0.1% [21]. In addition, if the frequency is above 50 kHz, such generators are treated as constant potential generators according to IEC standards [4].

To establish IEC radiation conditions, the generator voltage must be adjusted to match a specific PPV value given within the standard for each radiation condition. For this, the uncertainty of the PPV measurement must be below 1.5% or 1.5 kV (coverage factor  $k = 2$ ), whichever is larger. In addition, the ripple of the X-ray generator must be smaller than 10% for most IEC radiation conditions and smaller than 4% for mammography radiation conditions [5]. Also, ISO 4037 [21] gives strict requirements on the relative deviation of measured tube potential from the nominal value of the tube voltage measurement, which can be as small as 0.1%. According to this standard, the ripple of the generator must be smaller than twice the stated relative deviation. In contrast to IEC, the tube voltage in ISO 4037 is expressed in the tube potential.

## 2.8 Spectrometric practical voltage

Contrary to the invasive measurement of time variations of the tube voltage using a voltage divider, the non-invasive spectrometric method estimates the tube voltage from the time-integrated measurement of photons emitted from the anode after interactions of electrons there. The energy of accelerated electrons follows time variations of the tube voltage.

The presented method takes the end part of a measured spectrum resulting from interactions of photons in the detector and overlays it with a Monte Carlo-calculated detector spectrum initiated by monoenergetic electrons of the known energy  $E_0$  (or known distribution of energies, if more relevant). When an overlay is found, this energy is then the *end-point energy* ( $E_{\text{end}} = E_0$ ) of the given measured X-ray fluence spectrum. Therefore,  $E_{\text{end}}$  obtained this way is an average value of all  $E_{\text{end}}$  occurring in the real X-ray spectrum during the acquisition time of the detector spectrum. The quantity is the energy and the unit is the electronvolt, eV. Such a quantity is not utilized in standards describing reference radiation conditions. Instead, the standards use voltage quantities like the PPV or tube potential.

However,  $E_{\text{end}}$  is directly related to the mean voltage,  $U$ , because by definition 1 eV is the kinetic energy acquired by a single electron passing through an electric potential difference of 1 V in vacuum (equation (2.1)):

$$E_{\text{end}} = q \cdot U \quad (2.1)$$

where  $q$  is an electric charge. For a single electron,  $q$  is equal to an elementary charge, i.e.,  $q = 1 \text{ eV/V}$  in the appropriate physical unit.

Using equation (2.1), one can directly relate the known  $E_{\text{end}}$  to the X-ray tube voltage. This is why a quantity called *spectrometric practical voltage* has been defined, abbreviated as **SPV**. The SPV is the constant voltage (in kV) on the X-ray tube that resulted in  $E_{\text{end}}$  (in keV) obtained using the presented spectrometric method. As such,  $U = \text{SPV}$  in equation (2.1). The method determining the SPV is called the *spectrometric practical end-point method* and is abbreviated as **SPE method**. This method is detailed in section 2.10. When describing the result of the SPE method without the need to differentiate between energy and voltage, the terms end-point energy and SPV are interchangeable.

The SPV does not correspond to the kVp, because the SPE method does not look for the highest energy of counts in the detector spectrum. But it is similar in principle to the PPV, because both express some kind of average voltage. For this reason, the relation between the PPV and the SPV

was investigated. To do so, the fluence spectra N-60 (tube voltage 60 kV, mean energy 48 keV) and N-120 (120 kV, 100 keV) were calculated with the MCNP code (see section 2.10.2) for primary electrons with the energy uniformly distributed around 60 and 120 keV, respectively, and the edges of the energy interval defined by various voltage ripples from 0% to 10%. A waveform resulting in the uniform distribution of voltages was assumed. This can be an approximation in the case of high-frequency generators, which include a rectifier with a capacitor to smooth the voltage waveform. The PPV was calculated according to [23] and the kVp was obtained as the numerical value of the maximum electron energy. The SPV was determined from each detector spectrum calculated by MCNP for every such X-ray fluence spectrum in order to compare it with the PPV and kVp values. The results are summarized in section 3.4.

## 2.9 Preparation work

In preparation, additional characterization of the X-123CdTe detector was performed beyond the work done in [1–3], the aim being to find optimal measurement conditions and reduce the SPV uncertainty.

### 2.9.1 Charge carrier transport parameters and Gaussian energy broadening

The influence of the charge transport, collection, and recombination in the CdTe sensor on the detector response was described using an analytical model of the charge carrier transport (CCT). The CCT included effects of the carrier trapping modeled by a modified Hecht equation and the incomplete charge collection modeled by the carrier collection probability function. The energy resolution of the detector was expressed by the Gaussian energy broadening (GEB) of the collected charge. Analytical models of both effects were described in detail in [1]. A new estimation of the parameters of both analytical models was performed for the high-count-rate regime relevant for X-ray spectra measurements. The optimal maximum count rate was obtained from the analysis of the full width at half maximum (FWHM) of full-energy peaks (FEPs) in the detector spectra of selected radionuclides acquired at various count rates.

Where both effects are referred to in the following, they are jointly abbreviated as CCT+GEB.

### 2.9.2 Energy calibration

The accuracy of the energy calibration is crucial to ensuring the precision of the SPE method [8]. Detector energy calibration and the optimization of CCT+GEB parameters were performed simultaneously using sealed radionuclide sources. The selection of suitable radionuclides will be discussed later. In addition to the procedure applying CCT+GEB described in [1], new requirements were added to improve the calibration:

- The calibration was performed at the high-count-rate regime relevant for X-ray spectra measurements.
- The calibration was performed at the same temperature of the CdTe sensor as reached during X-ray spectra measurements.
- The calibration was performed with radionuclide sources providing the dead time and count rate corresponding to those achieved in X-ray spectra measurements.

Based on the spectrometer application, three different energy calibrations were considered: a) to determine the SPV at a high-count-rate regime ( $C_{Uhigh}$ ); b) to determine the SPV at a low-count-rate regime ( $C_{Ulow}$ ); and c) for visualization at a high-count-rate regime ( $C_{Vhigh}$ ).  $C_{Ulow}$  and  $C_{Uhigh}$  were determined by precisely pairing the energy of the primary photon with the channel related to this energy for each fitted FEP. Accurate energy calibration of this type is required for the SPV measurement and for the calculation of the detector response matrix needed for unfolding the primary photon fluence spectrum.  $C_{Ulow}$  can be easily determined, but  $C_{Uhigh}$  may be more difficult because the activity of radionuclide sources has to be sufficiently high to reach the requested detector count rate.

It should be noted that the FEP maximum does not correspond to the primary photon energy as presented in [1]. On the other hand,  $C_{Vhigh}$ , constructed by pairing the peak maximum with the energy of the primary photon, is suitable for the visual evaluation of peaks in the detector spectra.

The energy calibration should be checked with a suitable radionuclide source in close time proximity to the SPV measurement and, if the calibration has changed, a new energy calibration should be performed and used for the SPV evaluation. The sensor temperature during the energy calibration and the X-ray spectra measurements must agree within  $\pm 1$  K.

### 2.9.3 Efficiency calibration

The relative FEP detection efficiency in the relevant energy range was used as an independent quantity to check the values of parameters in the CCT+GEB models. The efficiency calibration was obtained from the same measurement as the energy calibration. The measurement geometry with radionuclide sources was replicated in the MC model. The detector spectra were simulated for the realistic photon emission spectra of the radionuclides used in the measurement. Photon energies and yields of the given radionuclides were taken from the DDEP database [24]. After application of the CCT+GEB adapted for the given count rate, the relative peak areas of selected FE peaks were compared to measurements. The agreement of the measured and the simulated relative peak areas supported the correctness of the modified values of the CCT+GEB parameters.

### 2.10 End-point energy

The proposed method for the spectrometric determination of the X-ray spectrum  $E_{end}$  and hence of the tube voltage is based on the comparison of the energy and shape of the end part of the measured detector spectra to those of the Monte Carlo-simulated detector spectra. No unfolding of the fluence spectrum is needed. Although unfolding can provide  $E_{end}$  of the fluence spectrum, this additional step, consisting of the unfolding and the coarser energy binning of the unfolded spectrum, increases the SPV uncertainty. The detector has to be properly energy calibrated according to the requirements stated in section 2.9.2. The Monte Carlo model of the detector must be available and validated. MC simulations do not require a detailed model of the spectrometer, but the CCT+GEB valid in the appropriate count-rate regime should be applied on the simulated detector spectrum. The steps of the SPE method demonstrated on N-series radiation qualities detailed in the subsequent sections are as follows:

1. Acquire a detector spectrum of N-series radiation quality.
2. Calculate the N-series fluence spectrum corresponding to the measured one using the appropriate filtration and the expected mean tube voltage, e.g., using the SpekPy software or a radiation transport Monte Carlo code. Do not apply the voltage ripple of the high-voltage generator

(unless it is intended) nor the Gaussian energy broadening of the detector.  $E_{\text{end}}$  of this kind of spectrum and the corresponding SPV are exactly known.

3. Use this calculated fluence spectrum as the particle source in the Monte Carlo simulation of the spectrometer response. Calculate the amplitude spectrum of counts in the sensor and simultaneously apply the CCT+GEB corrections. This yields the calculated detector spectrum.
4. Compare the end parts of the measured and the calculated detector spectra. If there is a difference, move the calculated spectrum by a constant energy to get the best agreement of the end part of the calculated spectrum with the measured spectrum.
5.  $E_{\text{end}}$  of the measured spectrum is then equal to the energy of monoenergetic electrons,  $E_0$ , used for the generation of the calculated fluence spectrum, corrected by the constant energy offset. The SPV is obtained from equation (2.1).

Any laboratory that has established in-beam X-ray spectrometry using an unfolding method should already have the tools required for SPV determination using the SPE method. These include a well-characterized detector in terms of energy calibration, energy resolution, and detection efficiency, as well as its validated Monte Carlo model, tools that are otherwise required for the calculation of the detector's response matrix.

### 2.10.1 Measurements

Since the SPV does not depend on additional filtration, any filtration could be selected. Obviously, suitable radiation quality should provide a high count rate at the highest part of the detector spectrum because low-energy photons do not improve SPV measurement and just needlessly increase the count rate. That is why the N-series radiation qualities [21] appear to be suitable for the SPE method, although for low kV and very high kV levels less filtered spectra might be more suitable in specific cases to achieve the desired count rate, e.g., when one aim is to perform measurement at low tube current. The N-series qualities are defined over the whole relevant kV range and are realized from 10 to 300 kV at CMI and from 10 to 400 kV at PTB. Moreover, thick additional filtration removes the low-energy parts of the spectra. For these reasons,  $E_{\text{end}}$  was in this study determined for N-series radiation qualities.

The relationship between the SPV obtained for N-series spectra and the nominal setting of the tube voltage is then valid for any other radiation quality realized at the same tube voltage and tube current.

The measurements were performed at a distance between the collimator front and the X-ray tube focus of 95.2 cm at CMI and 100 cm at PTB, i.e., the reference distances at the respective sites. See [2] for a detailed description of CMI's common setup for X-ray spectrometry measurements.

A set of three collimation disks with nominal diameters of 400  $\mu\text{m}$ , 1 mm, and 2 mm placed one after another at the front part of the collimator was used to decrease photon flux at the sensor. The tube current was tuned to obtain a detector count rate of roughly 13 000 imp/s. This was achieved for all N-series spectra except for N-10, N-200, N-250, and N-300 at CMI, where the target count rate could not be reached and ranged between 4500 and 8500 imp/s, and except for N-20, N-25, and N-30 at PTB, where the count rate reached approximately 2000 imp/s. Energy calibration valid for a count rate of 6000 imp/s was applied on the measured spectra described above; on all other spectra, energy calibration valid for a count rate of 13 000 imp/s was applied.

### 2.10.2 Calculation of primary X-ray spectra

Monte Carlo (MC) simulations of X-ray spectra were performed with a general-purpose radiation transport code MCNP<sup>®</sup> version 6.2 [25, 26] with electron library el03 [27] and electron-photon relaxation library EPRDATA14 [28] based on electron-photon interaction cross sections (EPICS) [29]. The modeled geometry included a tungsten anode inclined to the beam axis by an angle of  $21^\circ$ , inherent filtration (1 mm or 7 mm thick beryllium output window from the X-ray tube), monitoring chamber, and additional filtration corresponding to the given X-ray quality. Primary particles were monoenergetic electrons hitting the anode. The efficiency of the sampling of high-energy bremsstrahlung photons generated in the anode material was increased by setting the *bnum* parameter (*PHYS:E* card) to  $-20$  and by introducing the *BBREM* card [25]. The efficiency of the calculation of the energy distribution of photon fluence was further increased by using mesh weight windows (*WWG/WWP* cards). Details were presented in [3].

The N-series photon fluence spectra were calculated at the distance of 95.2 cm from the X-ray focus as in the CMI measurement. The  $E_0$  values of primary electrons were chosen to equal the expected value of  $E_{\text{end}}$ .

Alternatively to MC simulations, the fluence spectra can be obtained using the open-source software SpekPy [30–32]. The package is intended specifically for modeling X-ray tube spectra with the Python programming language utilizing a semi-empirical approach where parts of the spectrum model are based on physical theory but some parameters are adapted in order to bring predictions into conformance with experimental results.

Both described codes were previously validated and they provide shape of spectra in close agreement with experimental observations.

### 2.10.3 Calculation of detector spectra

The amplitude spectra of counts in the detector were calculated with the MCNP code (section 2.10.2). The MC model of the spectrometer described in [3] was updated to take account of recent modifications of the collimation and shielding [2]. Visualization of the spectrometer MC model is presented in figure 2.

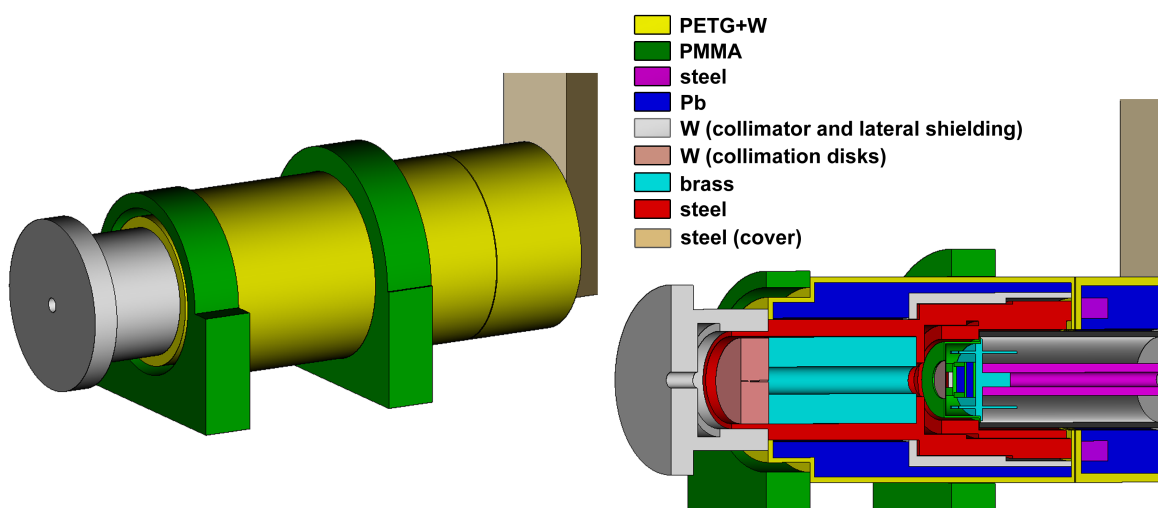


**Figure 2.** Visualization of the MC model of the spectrometer. The different materials are distinguished by color.

Photon energy distributions generated by MCNP simulations of the X-ray tube (section 2.10.2) were used as the primary particle source. The source particles started on a circle in front of the spectrometer. The scored quantity was the deposited energy in each of the sensor's 20 layers recorded event-by-event to a Particle Track (PTRAC) output file. Details on the simulated quantity and general settings of the simulations are provided in [3].

The PTRAC files were processed offline with a dedicated script in Matlab<sup>®</sup> software (The MathWorks<sup>®</sup>, U.S.A.) [3] to apply CCT+GEB using updated parameters valid in high-count-rate regime measurements (see section 3.1.3). This procedure resulted in calculated detector spectra with all corrections applied and ready for comparison to the measured spectra.

#### 2.10.4 Determination of end-point energy

The calculated detector spectrum (resulting from a fluence spectrum generated from electrons of the energy  $E_0$ ) and the corresponding measured spectrum were plotted onto the same graph (figure 3). The focus was placed on the high-energy part of the spectra and the GEB “tail” was not considered. Where necessary, a constant background was added to each bin of the calculated spectrum. If the end parts of the spectra were shifted relative to each other in energy, the energy of all bins of the calculated spectrum would be modified by a constant energy  $\Delta$  until agreement was achieved. No automated processes were used here. However, the minimum difference in the area of the two spectra bordered by the same pre-selected energies was sought as an indicator of the accuracy of the spectra overlay. When this minimum was found,  $E_{\text{end}}$  of the measured spectrum was equal to  $E_{\text{end}} = E_0 + \Delta$ .

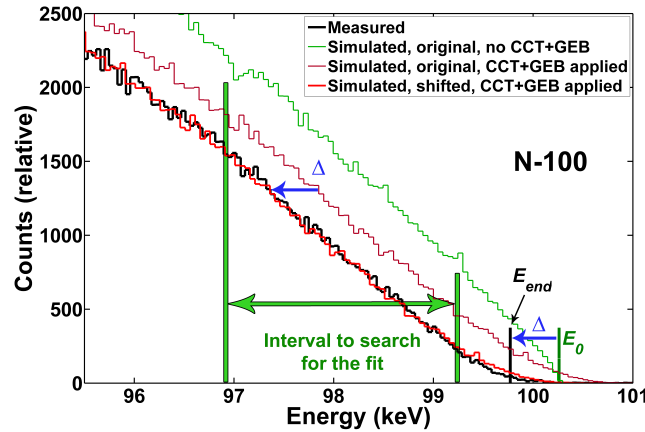


**Figure 3.** An example of the shift by a constant energy  $\Delta$  of the simulated detector spectrum of N-100 quality onto the measured spectrum to determine the end-point energy,  $E_{\text{end}}$ , of the measured spectrum. The aim was to obtain the best agreement of both spectra inside the energy interval bordered by the green lines close to the very end of the spectrum. The original detector spectrum resulted from the fluence spectrum generated by primary monoenergetic electrons of the energy  $E_0$ . In the presented case,  $E_0$  was not exactly 100 keV.

Typically, the match between the measured and the simulated detector spectrum was not complete over the entire interval from 0 keV to  $E_{\text{end}}$ . This was primarily due to the differences in real and modeled total filtration and the tube potential, as often only the nominal values were known. However, achieving exact agreement of shape over the whole spectra was not the pursued aim. The important aspect was the overlay of the high-energy parts only. Wherever possible, the chosen interval was placed at the end of the linear part of the spectrum in order to suppress the potential influence

of voltage ripple. If the voltage ripple is small, however, the simulated spectrum will follow the measured spectrum's non-linear tail as well.

### 2.10.5 Validation of the method

The presented method was validated by comparing the SPV derived from N-series detector spectra measured at PTB with the tube voltage readings previously obtained there with a calibrated voltage divider.

### 2.11 Influence of the tube current

Some studies suggest [33] that  $E_{\text{end}}$  depends on the tube current. This effect was tested with the 160 kV generator at CMI at a) 60 kV, where the highest tube current can be achieved; and b) at 150 kV, the practical tube voltage maximum used; and also with the 320 kV generator at a tube voltage of 200 kV. The influence of the detector count rate on the measured spectrum was minimized by keeping the count rate constant. This was achieved by adding metal sheets in front of the collimator aperture.

## 3 Results and discussion

### 3.1 Additional characterization of the detector

#### 3.1.1 Peak position and optimal count rate

A change in the position of the full-energy peaks, their shape, and their FWHM was observed in dependence of the detector count rate. The 59.5 keV FEP of  $^{241}\text{Am}$  and the 122 keV FEP of  $^{57}\text{Co}$  acquired at different count rates are presented in figure 4. The observed change in the position of the 59 keV and 122 keV peaks between acquisitions at 100 (or 700) and roughly 13 500 imp/s was 0.1 keV and 0.2 keV, respectively. For the accurate determination of  $E_{\text{end}}$ , it is necessary to account for these effects and perform the energy calibration at the count-rate regime relevant for  $E_{\text{end}}$  measurements.

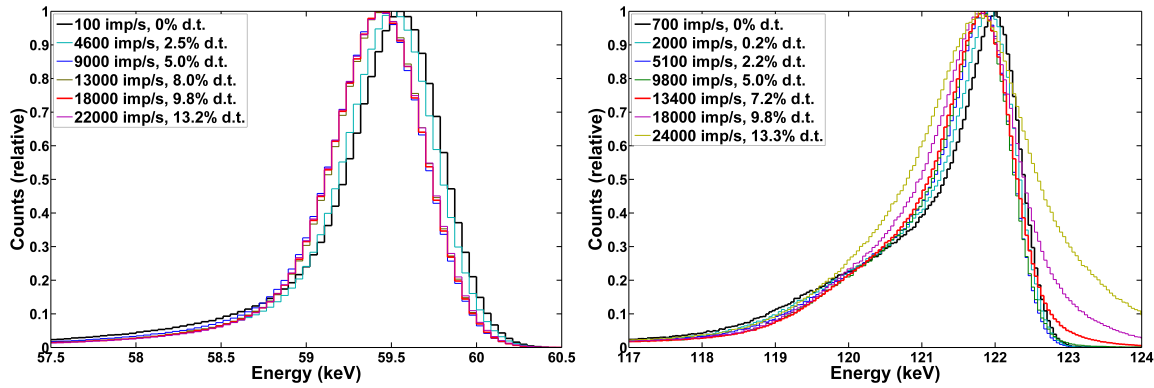


**Figure 4.** Position and shape of the 59 keV (left) full-energy peak of  $^{241}\text{Am}$  and the 122 keV full-energy peak of  $^{57}\text{Co}$  (right) acquired at various detector total count rates in pulses per second (imp/s), and the corresponding dead times (d.t.).

A summary plot of count-rate dependence of the FWHM of the FEP at 59.3 keV of the characteristic  $K\alpha_1$  line of tungsten in RQR10 radiation quality, 59.5 keV of  $^{241}\text{Am}$  radionuclide, and 80 keV of  $^{133}\text{Ba}$  radionuclide (fit of the higher energy peak of the doublet) is depicted in figure 5. The FWHM is constant up to a certain count rate and then increases along with the count rate. Although the

FWHM is also influenced by other parameters besides the count rate and the energy of the FE peak, for X-ray beam spectrometry it is important how the FWHM changes in the X-ray spectra, especially the tungsten K-lines at roughly 58 keV and 67 keV if a tungsten anode is used. Therefore, based on the results, the optimal maximum total count rate in CMI X-ray spectrometry measurements was established to be 13 000 imp/s. The detector energy calibration was performed at this count rate and it was, where achievable, the target count rate in  $E_{\text{end}}$  measurements. However, if no peaks occur in the X-ray spectrum (i.e., typically spectra generated with the tube voltage < 70 keV) and the goal of the measurement is not to determine the SPV, it was decided that the detector spectrum can be acquired at up to the double count rate. No differences were observed in the shape of such spectra acquired at 13 000 imp/s and at the double count rate. The stated count rates are valid for the detector setting presented in section 2.1. A different optimal count rate may be obtained for another detector of the same type or with another setting.

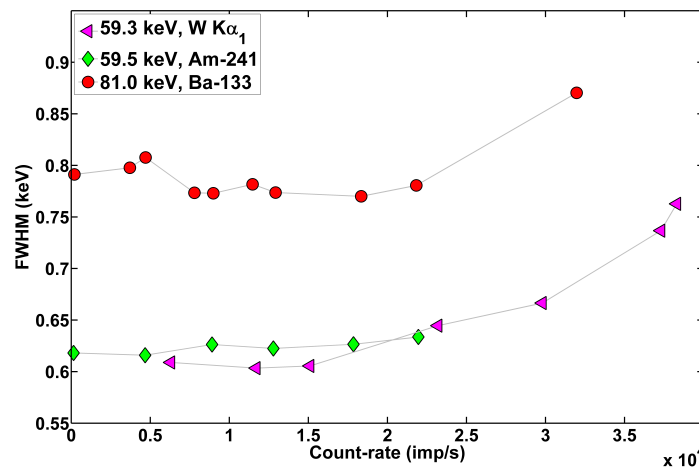


**Figure 5.** The full width at half maximum (FWHM) of selected full-energy peaks as a function of the total count rate in pulses per second (imp/s) for the used detector and its applied setting. The FWHM here represents the width of the whole peak taking into account the combination of GEB and CCT effects; it does not correspond to the FWHM caused solely by the detector energy resolution, as described in [1], which is lower. The lines are included to aid visualization.

### 3.1.2 Dead-time dependence on count rate and energy

The dead time rises with increasing count rate, which also results in a change of the FEP's shape and position as shown in section 3.1.1. However, the dead time also depends on the energy deposited at one interaction and the position of the interaction in the sensor. For the constant count rate, high energy deposition results in higher dead times because of the prolonged charge collection at the electrodes. It also has an influence on the FEP's shape. This is demonstrated in figure 6, which shows the 344 keV FEP of  $^{152}\text{Eu}$  measured at the same count rate but with the low-energy photons filtered by various metal materials: 6 mm thick aluminum, 2 mm thick brass + 2 mm thick tin, and 4 mm thick lead. The observed change of the peak position was roughly 0.4 keV.

On the basis of this result, a study was made of the relationship between the dead time and the detector total count rate for various X-ray qualities and radionuclide sources. Measurements at various count rates were performed in X-ray qualities and radionuclide photon fields. The X-ray qualities used

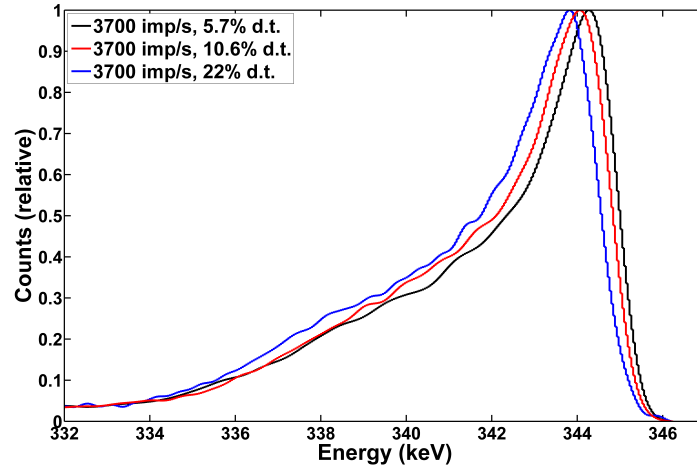


**Figure 6.** Position and shape of the 344 keV FE peak of  $^{152}\text{Eu}$  at the same detector total count rate but with different filtration of  $^{152}\text{Eu}$  low-energy photons: acquisitions were obtained for filtrations made of 6 mm thick aluminum (5.7% dead time, d.t.), 2 mm thick brass + 2 mm thick tin (11%), and 4 mm thick lead (22%). The spectra were smoothed and normalized to the peak maximum to highlight the differences.

were N-60 (tube voltage of 60 kV, mean energy in fluence 48 keV), N-200 (200 kV, 164 keV), N-300 (300 kV, 252 keV), and an ad-hoc 150 kV quality with N-60 additional filtration (150 kV, 95 keV). The radionuclide sources were  $^{241}\text{Am}$ ,  $^{133}\text{Ba}$ ,  $^{57}\text{Co}$ , and  $^{152}\text{Eu}$ . The latter two were encapsulated in a steel cover that absorbed low-energy photons. The dead time as a function of the total count rate is depicted in figure 7. A similar relationship was observed for all tested spectra except for that of  $^{152}\text{Eu}$ . The deviation seen with this radionuclide was caused by low-energy photons being absorbed in the encapsulation, resulting in a much higher average energy of the emitted photons (average energy of photons above 10 keV was 500 keV, maximum energy roughly 1.5 MeV) compared to the X-ray qualities (maximum photon energy of 300 keV) and other radionuclides (the average energy of photons above 10 keV of  $^{241}\text{Am}$ ,  $^{57}\text{Co}$ , and  $^{133}\text{Ba}$  was roughly 57 keV, 115 keV, and 156 keV, respectively, and the maximum energy was roughly 60 keV, 136 keV, and 365 keV, respectively).

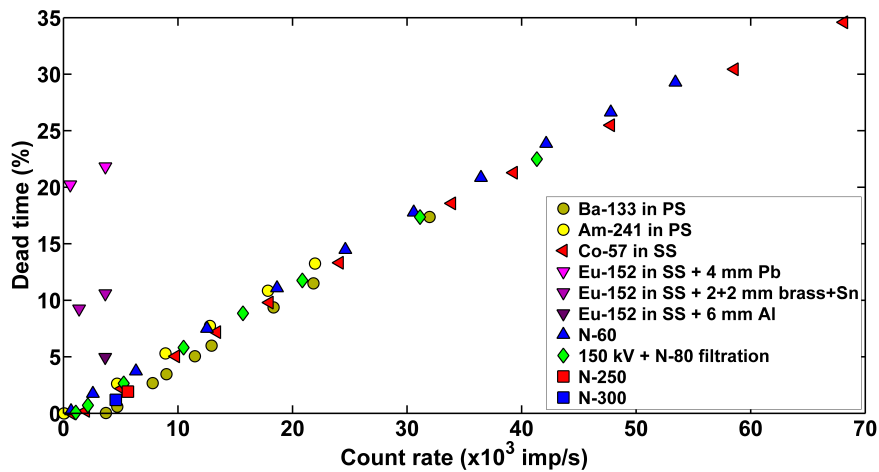


**Figure 7.** Detector dead time as a function of the detector total count rate for various X-ray qualities and radionuclide sources. PS stands for polystyrene, SS for stainless steel.

The detector response should be the same under irradiations by calibration radionuclide sources and by X-ray beams. Therefore,  $^{241}\text{Am}$ ,  $^{133}\text{Ba}$ , and encapsulated  $^{57}\text{Co}$  sources appear to be suitable radionuclides for accurate X-123CdTe detector energy calibration in a high-count-rate regime. On the other hand, encapsulated  $^{152}\text{Eu}$  radionuclides should be avoided, if possible, because its use may result in the energy calibration and energy resolution differing from the ones observed in X-ray spectrometry at the same count rate.

For the energy range relevant to X-ray beam spectrometry, the dependence of the dead time on the mean photon energy for selected X-ray qualities and radionuclide sources is presented in figure 8. Data was acquired at a count rate of  $(13\,500 \pm 500)$  imp/s.

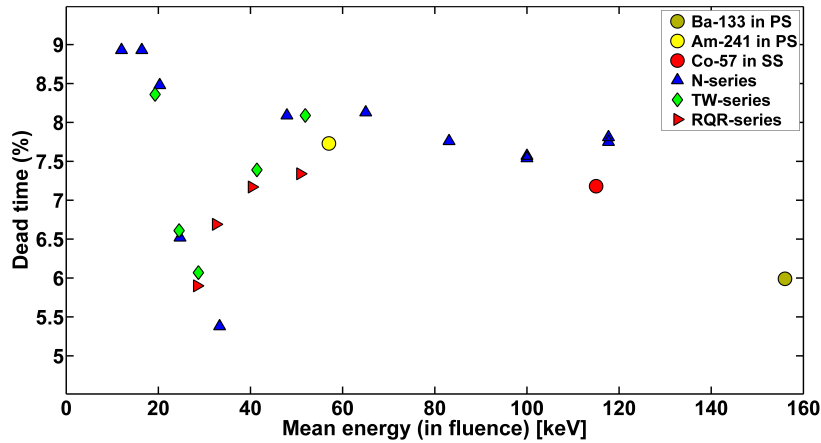


**Figure 8.** Dead time as a function of the mean photon energy (in fluence) at the same count rate of  $(13\,500 \pm 500)$  imp/s for selected X-ray qualities and radionuclide sources.

As a result, the energy calibration of the detector valid for the measurement of X-ray spectra at a high-count-rate regime of roughly 13 000 imp/s was performed with  $^{241}\text{Am}$ ,  $^{57}\text{Co}$ , and  $^{133}\text{Ba}$  radionuclides. FEPs with the following photon energies were used: 13.9, 26.3, and 59.5 keV of  $^{241}\text{Am}$ , 122.1 keV of  $^{57}\text{Co}$ , and 31.0, 81.0, 160.6, 223.2, 276.4, and 302.9 keV of  $^{133}\text{Ba}$ . The latter radionuclide is very suitable for such energy calibration because it covers most of the energy range of interest.

### 3.1.3 Charge carrier transport parameters and energy resolution

The FEP shape in the detector spectrum is influenced by the detector count rate as was demonstrated in figure 4. This was partly caused by the change in the CCT in the sensor, which is manifested as the change of the FEP width and of the shape of the left-hand side tailing of the FEP peak. The comparison of the 302 keV  $^{133}\text{Ba}$  FEP measured at a low-count-rate regime at 100 imp/s and at a high-count-rate regime at 13 000 imp/s in figure 9 (left) demonstrates the extent of the peak tailing effect. An example of the change of peak width in the measured X-ray spectrum is the broadening of tungsten  $K\alpha$  and  $K\beta$  peaks presented in figure 9 (right). This is the characteristic of the detector and is not related to the characteristic of the X-ray generator (see 3.3 and 3.5). The influence of the count rate on the FWHM of the selected FE peaks was also presented in figure 5.

Thus, the new values of the CCT+GEB parameters valid in the high-count-rate regime were evaluated from the spectra of  $^{241}\text{Am}$ ,  $^{57}\text{Co}$ , and  $^{133}\text{Ba}$  radionuclides, all acquired in the high-count-rate regime of approximately 13 000 imp/s. The measured FE peaks (see section 3.1.2) were fitted as

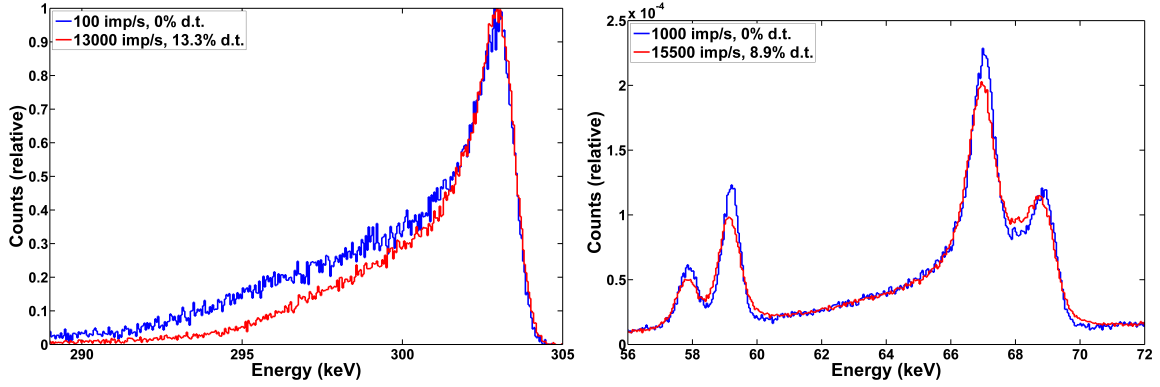


**Figure 9.** 302 keV full-energy peak of  $^{133}\text{Ba}$  (left) and tungsten fluorescence lines in the X-ray spectrum (right) measured in low and high-count-rate regimes. The count rate in pulses per second (imp/s) and the dead time (d.t.) are provided in the graph legends.

detailed in [1] and the parameters of the fitting curve were iterated until a satisfactory agreement was achieved for all fitted peaks for the same set of CCT+GEB parameters, thereby also fulfilling the requirement of agreement between the measured and the simulated relative detection efficiencies (section 3.1.4). In fact, only the GEB parameters and the mean drift length for holes,  $\lambda_h$ , were modified compared to the calibration in the low-count-rate regime [1]. The relative change of the FWHM of the FE peaks was about +10% across the whole energy range compared to the values presented in [1]. The  $\lambda_h$  value was changed from 1.3 cm to 1.8 cm. An example of the fit of 59.5 keV and 276.4 keV FE peaks is presented in figure 10.

The described analytical corrections applied to the simulated data are valid for the given detector setting. Modification of the setting may change the detector response and influence CCT+GEB parameter values.

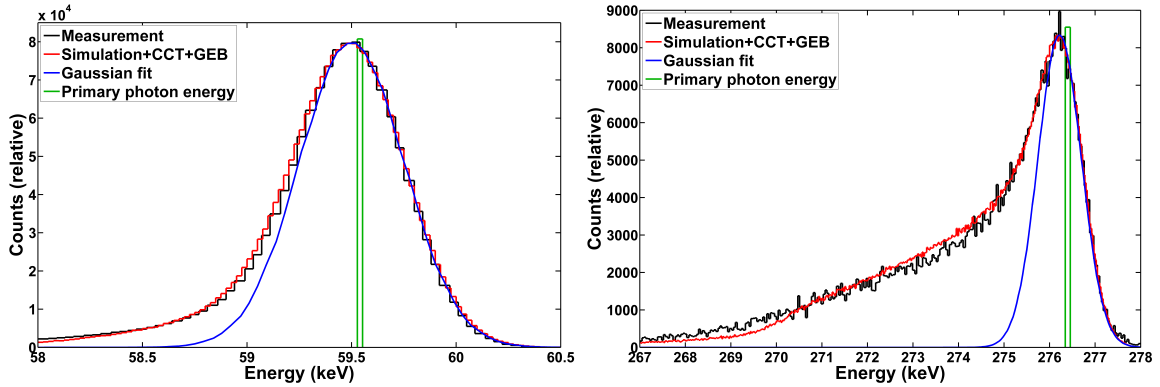


**Figure 10.** Example of the measured (black) 59.5 keV ( $^{241}\text{Am}$ ; left) and 276.4 keV ( $^{133}\text{Ba}$ ; right) full-energy peaks, their full fit based on Monte Carlo simulated detector response with applied CCT+GEB (red), the Gaussian fit defining the energy resolution only (blue), and the energy of the initial photon (green). A shift of the peak maximum to lower energy compared to the energy of monoenergetic photons can be observed, which accounts for the difference between the energy calibrations used for  $E_{\text{end}}$  measurement and for detector spectra visualization.

### 3.1.4 Efficiency calibration

The measured and simulated relative detection efficiencies obtained for the selected FE peaks of  $^{241}\text{Am}$  and  $^{133}\text{Ba}$  are presented in table 1. The satisfactory agreement confirmed the values of the CCT+GEB parameters obtained as described in section 3.1.3.

**Table 1.** Comparison of the measured ( $\text{RE}_{\text{EXP}}$ ) and simulated ( $\text{RE}_{\text{MC}}$ ) relative detection efficiencies for FEP of  $^{241}\text{Am}$  and  $^{133}\text{Ba}$  radionuclides. Efficiencies are related to the lowest photon energy used for each radionuclide. The region of interest (ROI) of the FEP was the same for both the measured and the simulated spectra and was selected to include the peak and its lefthand side tailing.

Photon energy (keV)	ROI $E_{\text{min}}$ (keV)	ROI $E_{\text{max}}$ (keV)	$\text{RE}_{\text{EXP}}$	$\text{RE}_{\text{MC}}$	$\text{RE}_{\text{MC}}/\text{RE}_{\text{EXP}} - 1$
<b><math>^{241}\text{Am}</math></b>					
<b>26.3</b>	25.5	26.9	1	1	-
<b>59.5</b>	56.0	60.8	0.894	0.907	1.4%
<b><math>^{133}\text{Ba}</math></b>					
<b>31.0</b>	29.8	31.7	1	1	-
<b>81.0</b>	75.0	82.0	0.829	0.839	1.2%
<b>276.4</b>	267.0	277.6	0.0447	0.0448	0.3%
<b>302.9</b>	294.0	304.5	0.0335	0.0357	6.7%

### 3.1.5 Energy calibration

The shift of the FEP maximum to lower energy, which accounts for the difference between the calibration for visualization,  $C_V$ , and that for unfolding and  $E_{\text{end}}$  measurement,  $C_U$ , can be observed in the peaks depicted in figure 10. The difference between  $C_{\text{Uhigh}}$  and  $C_{\text{Vhigh}}$  in a high-count-rate regime and between  $C_{\text{Uhigh}}$  and  $C_{\text{Ulow}}$  in different count-rate regimes is shown in figure 11. Systematic error can reach up to 0.2 keV if an improper energy calibration is used. Moreover, in the given calibration the absolute difference between each calibration point and its quadratic fit was less than 0.05 keV.

### 3.1.6 Impact on parameters of unfolded X-ray spectra

The main goal of X-ray spectrometry is to accurately determine the primary photon fluence energy distribution, which is then usually used to calculate its mean energy, half-value layers, conversion coefficients to dosimetric quantities, etc. Previous sections summarized a study of the detector response under real measurement conditions and proposed methods for its accurate description. This section presents a summary comparison of parameters of selected unfolded X-ray fluence spectra to provide an overview of systematic errors if a detector effect is not taken account of during measurement or in data evaluation. The comparison is demonstrated on the measured N-series, RQR-series, and TW-series radiation qualities realized at CMI. For the sake of this comparison, the parameters were calculated from X-ray spectra unfolded with the following response matrices (RMs):

- RM1: reference RM - high-count-rate regime, CCT+GEB applied

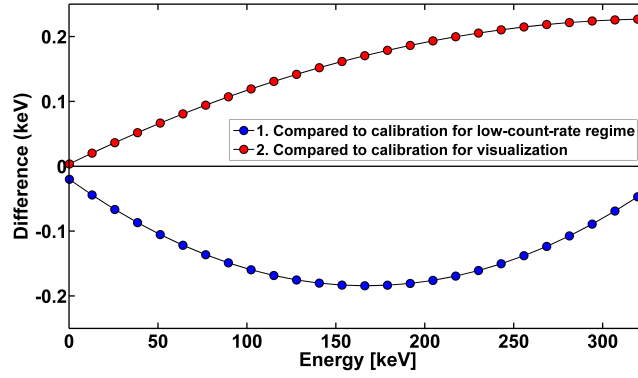


**Figure 11.** The difference between values of energy calibration curves:  $C_{Ulow}$ ,  $C_{Uhigh}$ , and  $C_{Vhigh}$  are, respectively, the calibration for unfolding and  $E_{end}$  measurement at a low-count-rate regime, for unfolding and  $E_{end}$  measurement at a high-count-rate regime, and for visualization at a high-count-rate regime. 1. is the difference  $C_{Ulow} - C_{Uhigh}$ , 2. is the difference  $C_{Vhigh} - C_{Uhigh}$ .

- RM2: CCT neglected - high-count-rate regime, GEB applied
- RM3: CCT+GEB neglected - high-count-rate regime, CCT+GEB not applied
- RM1b: as RM1, but energy calibration for visualization was used
- RM1c: as RM1, but energy calibration for low-count-rate regime was used

The following quantities were compared: the mean energy of fluence spectrum (table 6); the first half-value layer (HVL) in Al or Cu (table 7); the homogeneity coefficient in Al or Cu (table 8); the conversion coefficient from air kerma to the dose equivalent  $H_p(10)$  in the ICRU slab phantom at an angle of radiation incidence of  $0^\circ$ ,  $h_{pK}(10; 0^\circ)_{slab}$  (table 9); and the conversion coefficient from air kerma to the directional dose equivalent  $H'(0.07)$  at an angle of radiation incidence of  $0^\circ$ ,  $h'_K(0.07; 0^\circ)$ , (table 10). The reader is referred to [21] and [34] for definitions of these quantities. The tables are presented in the appendix.

The lowest systematic error from the studied variants was achieved when the energy calibration for visualization was used instead of that for unfolding. The obtained relative difference (RD) to the reference value was typically within 0.3% for all quantities. In general, larger RDs resulted for quantities with a larger dependence on the photon energy, e.g., HVL and  $h_{pK}(10; 0^\circ)_{slab}$ .

RDs similar to those in the previous case were achieved when the energy calibration was performed in a low-count-rate regime instead of a high-count-rate regime corresponding to the count rate during detector spectra acquisition. The systematic error was within 0.5%, except for low-energy X-ray qualities with the mean energy below roughly 20 keV; here, the error was as high as a few percent.

Larger systematic errors were obtained when the CCT+GEB were not applied. The largest influence was exerted by the CCT. The RDs for the mean energy and the  $h'_K(0.07; 0^\circ)$  varied within 1% (except for the lowest energy X-ray qualities), but for other quantities the RD was typically a few percent and reached up to 17% for very low-energy X-ray qualities.

Although the relative differences presented in the tables in appendix are typically very small, for some combinations of quantities and X-ray spectra, the quantity calculated from the fluence spectrum unfolded with the response matrix that does not take account of CCT, GEB, or accurate energy calibration may produce significant systematic uncertainty.

The presented variants RM2 and RM3 of the reference response matrix RM1 do not influence the  $E_{\text{end}}$  value because the described method for  $E_{\text{end}}$  estimation does not use unfolded spectra. Only the detector energy calibration, considered in RM1b and RM1c, influences the resulting  $E_{\text{end}}$  value.

## 3.2 End-point energy

### 3.2.1 Uncertainty assessment

The uncertainty components assumed in  $E_{\text{end}}$  determination are presented in table 2. The final combined uncertainty evaluated for N-series qualities at CMI is summarized in table 4. The uncertainty components were summed quadratically. The uncertainty estimation does not include a potential dependence of  $E_{\text{end}}$  on the X-ray tube current. The effect of the voltage ripple and the influence of the tube current are discussed in sections 3.3 and 3.5, respectively. If the stability of the energy calibration is checked shortly before or after  $E_{\text{end}}$  measurement, or if the  $E_{\text{end}}$  measurement is performed at the same count rate as the energy calibration, the respective uncertainties expressed in table 2 can be reduced accordingly and the combined uncertainty would decrease.

**Table 2.** Uncertainty budget for the end-point energy ( $E_{\text{end}}$ ) values.

	Uncertainty component	Uncertainty, $k = 1$
	Energy calibration curve	0.06 keV
	Difference between energy calibration for high-count-rate regime and at the used count rate	0.1 keV
	Energy calibration stability over time (checked shortly before or after $E_{\text{end}}$ measurement)	0.05 keV
	CCT and energy resolution	0.01% of $E_{\text{end}}$
	Overlay of simulated and measured detector spectrum end part	0.10% of $E_{\text{end}}$

The IEC 61267 standard [5] defines radiation conditions for the tube voltage ranging from 40 to 150 kV. The voltage in terms of the PPV should be known with an uncertainty below 1.5% or 1.5 keV, whichever is larger, at  $k = 2$ . The uncertainty of the SPE method and hence the SPV uncertainty is lower than the requirement across the entire voltage range. Although the requirement is fulfilled, this is not sufficient for the establishment of IEC radiation conditions if the wording of the standard is followed literally, since non-invasive methods are not allowed in determining the tube voltage.

The ISO 4037 standard [21] has various requirements on the maximum relative deviation between the measured and the nominal tube potential, depending on the quantity, angle of radiation incidence, and radiation quality. The SPV uncertainty fulfills the requirements on all such spectra and quantities realized with tube potentials of 40 kV and above (except for  $h_{pK}(0.07; 90^\circ)$ ). A specific characterization of the detector response in the low-energy region would be needed for the realization of lower kV spectra and quantities to decrease the uncertainties and fulfill ISO 4037 requirements. A suitable approach here would combine individual energy calibration in the low-energy range, measurement and energy calibration performed at the same count rate, and energy calibration realized shortly before or after the  $E_{\text{end}}$  measurement. This approach is discussed in further detail in section 3.4.

### 3.2.2 Validation

An example of the overlay of the measured and the calculated detector spectra of N-80 and N-300 radiation qualities realized at PTB is depicted in figure 12. The plots also include a linear fit of the straight part of the high-energy end of the spectra, which is often used in literature as a quick method for obtaining  $E_{\text{end}}$ , e.g., in [8] or the obsolete ISO 4037:1996 [16].

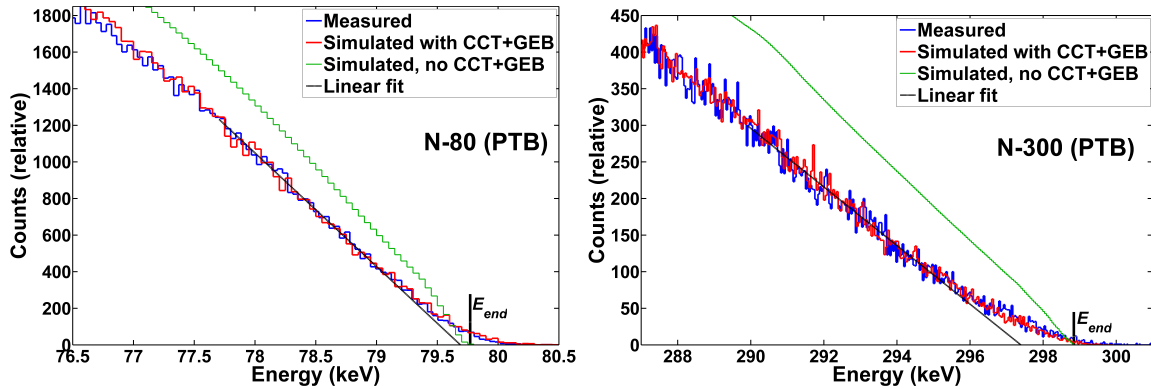


**Figure 12.** High-energy part of the calculated N-80 and N-300 detector spectra overlaid onto the corresponding spectra measured at PTB. Linear fitting of the straight part of the high-energy end of the measured spectra is used to determine the end-point energy obtained by the classic approach. A smoothed simulated detector spectrum without applied CCT+GEB is also shown and indicates the end-point energy obtained using the SPE method.

A summary comparison of the voltage divider reading and the SPV derived from X-ray spectrometry measurement is provided in table 3.

The differences between the voltage divider reading and the SPV varied between 0.1% and 0.8% relatively, and in absolute terms between 0.15 keV and 1.16 keV, as also visualized in figure 13. The spectrometry results were lower. The differences were smaller than their expanded uncertainties ( $k = 2$ ) except for the N-250 and N-300 qualities. At tube voltages above roughly 150 kV, the difference showed a dependence on the nominal tube voltage, something that has not yet been explained and is the subject of further investigation. In general, however, good agreement was obtained between the SPV and the voltage divider readings.

### 3.2.3 End-point energy measured at CMI

An example of the comparison of the high-energy end of the detector spectra measured at CMI and the fitted calculated detector spectra is presented in figure 14. The linear fit of the spectra end part, used as one of the two methods in the previous work [3], is also shown. The results obtained for all CMI N-series qualities are summarized in table 4.

For the 160 kV X-ray tube, the nominal tube voltage was about 0.9 kV lower than the SPV across the whole energy range of this instrument. Larger differences were observed for the 320 kV X-ray tube as presented in figure 13. The nominal tube voltage applied for N-series qualities and presented in table 4 had been set long before this study was initiated, which is why the SPV values do not agree with the expected values for N-series qualities. The differences obtained at CMI were larger than those resulting from the measurements at PTB because the determination of the tube voltage with a voltage divider at PTB is more accurate than the procedure used by CMI.

**Table 3.** Spectrometric practical voltage, SPV, and the end-point energy from a linear fit,  $E_{\text{end}}$  linear, obtained from N-series radiation qualities measured at PTB (450 kV generator) compared to the voltage divider reading ( $U_{\text{VD}}$ ). Uncertainties are stated at  $k = 1$ . <sup>(1)</sup> See table 2 for the uncertainty budget. <sup>(2)</sup> Relative difference between the SPV and the voltage divider reading,  $U_{\text{VD}}$ :  $\text{RD} = \text{SPV}/U_{\text{VD}} - 1$ . <sup>(3)</sup>  $E_{\text{end}}$  from the linear fit.

Quality	Tube current (mA)	Detector count rate (imp/s)	Voltage divider, $U_{\text{VD}}$ (kV)	SPV <sup>(1)</sup> (kV)	RD <sup>(2)</sup> (%)	$E_{\text{end}}$ linear <sup>(3)</sup> (keV)
N-20	5.9	1 400	20.00 ± 0.05	19.85 ± 0.13	−0.75 ± 1.26	19.89
N-25	5.9	2 000	25.00 ± 0.05	24.80 ± 0.13	−0.80 ± 0.52	24.86
N-30	5.9	1 700	30.00 ± 0.05	29.82 ± 0.13	−0.60 ± 0.43	29.89
N-40	10	11 500	40.00 ± 0.05	39.83 ± 0.13	−0.43 ± 0.33	39.91
N-60	3.5	14 300	60.00 ± 0.05	59.81 ± 0.14	−0.32 ± 0.23	59.86
N-80	5	13 100	80.00 ± 0.05	79.77 ± 0.15	−0.29 ± 0.19	79.69
N-100	15	13 700	100.00 ± 0.05	99.77 ± 0.16	−0.23 ± 0.16	99.56
N-120	20	13 600	120.00 ± 0.05	119.86 ± 0.18	−0.12 ± 0.15	119.49
N-150	4	14 200	150.00 ± 0.05	149.80 ± 0.20	−0.13 ± 0.13	149.14
N-200	15	8 200	200.00 ± 0.05	199.65 ± 0.24	−0.17 ± 0.12	198.72
N-250	15	5 700	250.00 ± 0.05	249.36 ± 0.28	−0.26 ± 0.11	248.16
N-300	15	5 600	300.00 ± 0.05	298.84 ± 0.33	−0.39 ± 0.11	297.39

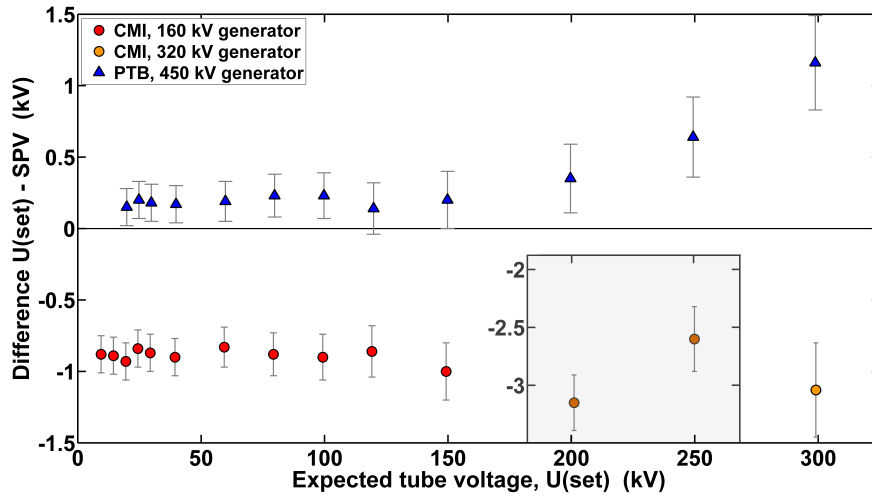


**Figure 13.** The difference between the SPV derived by the SPE method and a) for CMI spectra, the expected tube voltage,  $U(\text{set})$ , set on the 160 kV (red) and the 320 kV (orange) X-ray generator, or b) for PTB spectra, the expected tube voltage,  $U(\text{set})$ , equal to the voltage divider reading corresponding to the radiation conditions for N-series qualities (blue). The inset shows data points lying outside of the y-axis range of the main plot. The error bars show uncertainties at  $k = 1$ .

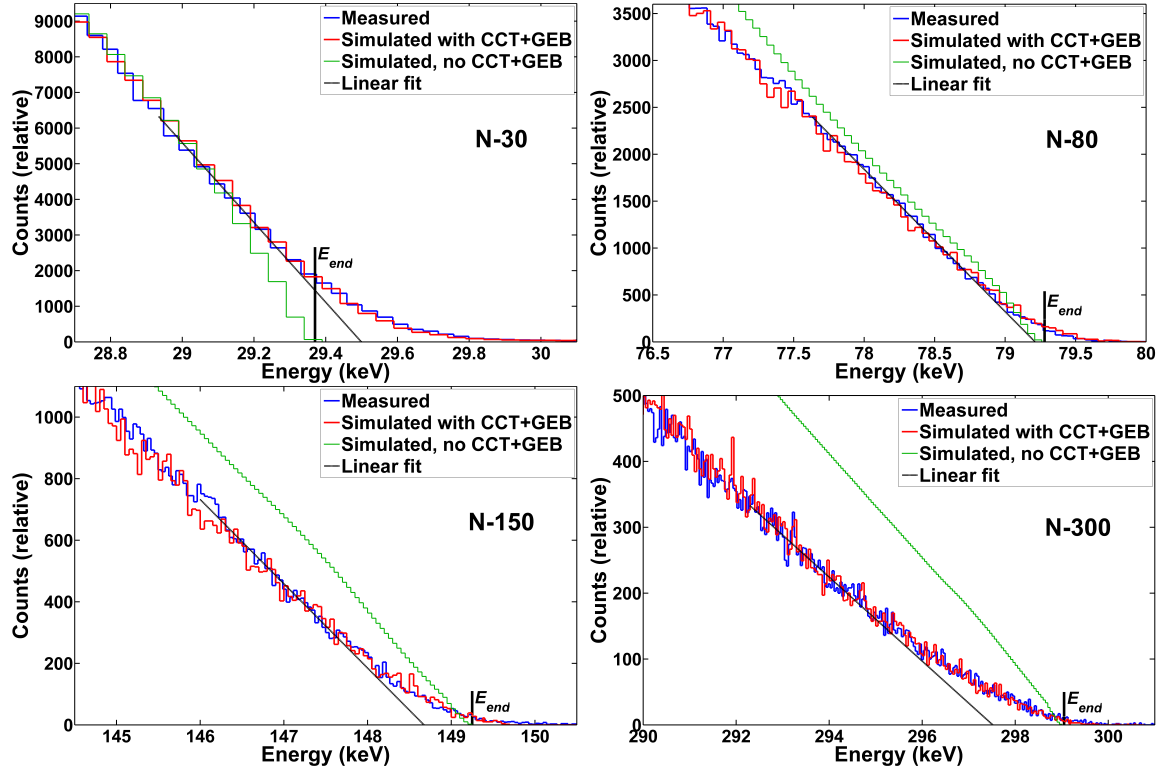


**Figure 14.** Simulated high-energy part of detector spectra overlaid on the spectra measured at CMI. See figure 12 for details.

**Table 4.** Spectrometric practical voltage,  $SPV$ , and end-point energy from a linear fit obtained from N-series radiation qualities measured at CMI. Uncertainties are stated at  $k = 1$ . <sup>(1)</sup> See table 2 for the uncertainty budget.

Generator	Quality	Tube current (mA)	Detector count rate (imp/s)	Nominal tube voltage (kV)	$SPV^{(1)}$ (kV)	$u(SPV)^{(1)}$ (%)	$E_{end}$ from linear fit (keV)
160 kV	N-10	28	4 500	8.57	$9.45 \pm 0.13$	1.27	9.62
	N-15	26	13 200	13.56	$14.45 \pm 0.13$	0.85	14.62
	N-20	9	13 700	18.55	$19.48 \pm 0.13$	0.64	19.56
	N-25	6.5	13 300	23.53	$24.37 \pm 0.13$	0.52	24.46
	N-30	7	13 100	28.50	$29.37 \pm 0.13$	0.43	29.50
	N-40	8	13 100	38.50	$39.40 \pm 0.13$	0.33	39.53
	N-60	2.5	13 400	58.45	$59.37 \pm 0.14$	0.23	59.45
	N-80	4	13 600	78.40	$79.28 \pm 0.15$	0.19	79.21
	N-100	11	13 000	98.36	$99.26 \pm 0.16$	0.16	99.04
	N-120	15	13 200	118.32	$119.18 \pm 0.18$	0.15	118.88
	N-150	3	14 000	148.25	$149.25 \pm 0.20$	0.13	148.67
320 kV	N-200	12	7 900	198.10	$201.15 \pm 0.24$	0.12	200.22
	N-250	12	5 600	248.00	$250.60 \pm 0.28$	0.11	249.34
	N-300	10	4 600	297.90	$299.05 \pm 0.33$	0.11	297.52

$E_{\text{end}}$  obtained from the linear fit slightly differed from values yielded by the SPE method, as shown in figure 15. The assumed reason is the Gaussian energy broadening of spectra to higher energies, which is not corrected for when applying the linear fit. Up to about 60 kV, the SPE method provided  $E_{\text{end}}$  values that were consistently lower by roughly 0.15 keV. Above 60 kV, the effect of the shift of FEP maximum to lower energies began to dominate due to the CCT. The linear fit did not take this effect into account and hence provided lower  $E_{\text{end}}$  values. However, up to 100 kV both methods agreed within 0.2 keV.

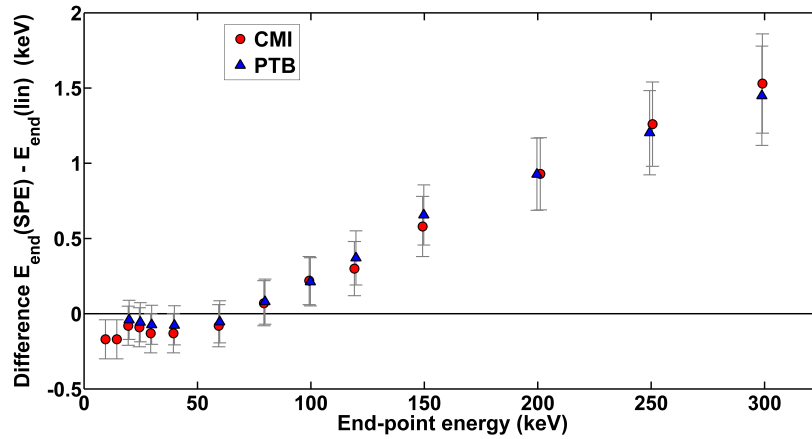


**Figure 15.** Difference between the values of the end-point energy obtained by the SPE method,  $E_{\text{end}}(\text{SPE})$ , and by linear regression,  $E_{\text{end}}(\text{lin})$ . Error bars consist of the uncertainty of  $E_{\text{end}}(\text{SPE})$  only. Two independent data sets obtained from N-series detector spectra are presented: measurements at CMI (red) and at PTB (blue). The close agreement between the two datasets stems from the similarity of N-series qualities realized at both laboratories.

### 3.3 Influence of voltage ripple

The effect of the voltage ripple on the shape of Monte Carlo-simulated N-60 and N-120 X-ray fluence spectra is demonstrated in figure 16. The ripple causes blurring of the far end part of the spectrum. The higher the ripple, the larger is the tail at the end of the detector spectrum.

In the measured spectrum, the effect of the voltage ripple was summed with the effect of the detector energy resolution, resulting in a wider tail at the end of the spectrum. That is why, in contrast to the fluence spectra, the detector spectra were indistinguishable from the spectrum without the ripple if the ripple did not exceed approximately 0.5% for the given detector type and setting. This is illustrated in figure 17, where only those detector spectra with a ripple of 1% and higher visually differ from the zero-ripple spectra. Moreover, detector spectra with a ripple of up to about 2% yielded the same  $E_{\text{end}}$  value. This is because the fit was performed using the calculated spectrum assuming zero ripple and taking into account the high-energy end of the spectrum but not its far end where the influence of such small ripples occurs, as demonstrated in figure 17. Therefore, the fit was the same for all such non-zero-ripple spectra. The spectra influenced by larger ripple could not be fitted with the zero-ripple spectrum, and a different calculated spectrum would be needed that considers the waveform of the high-voltage generator. As discussed in the following section, this is not the case with the high-frequency generators used at CMI, as visualized in figure 14. That is why the fitting of the spectra influenced by larger ripple will not be investigated further in this study.

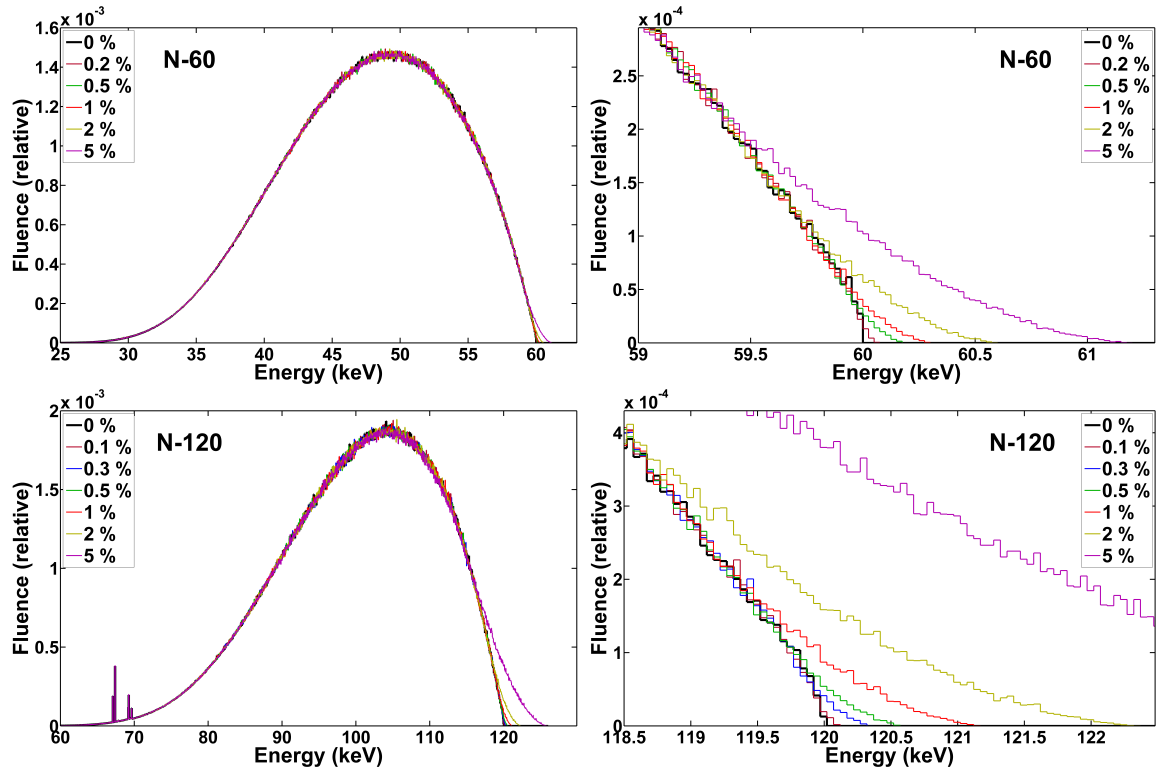


**Figure 16.** MC-simulated N-60 (60 kV; top row) and N-120 (120 kV; bottom row) X-ray fluence spectra generated with the tube voltage with various voltage ripples. Uniform distribution of the tube voltage around its nominal value was assumed. The spectra were normalized to unit area.

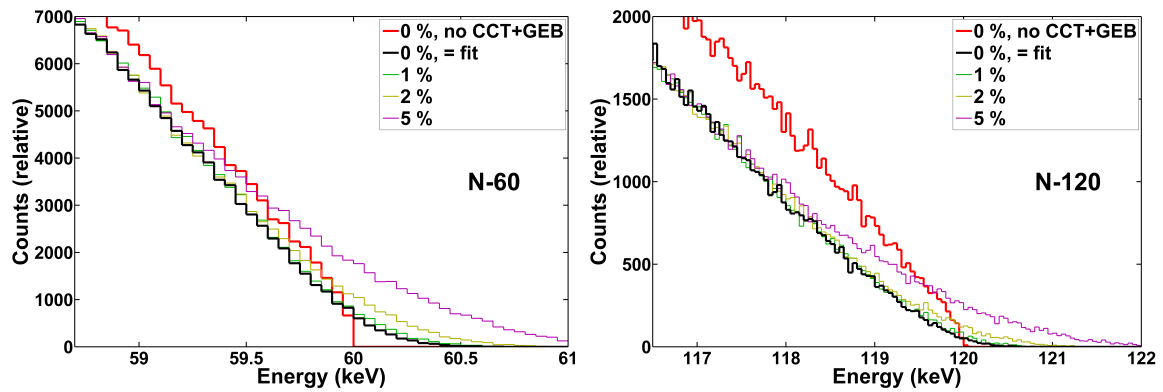


**Figure 17.** MC-simulated N-60 (60 kV, left) and N-120 (120 kV, right) detector spectra for various voltage ripples calculated from the fluence spectra depicted in figure 16. The spectrum for zero ripple is the one used in this paper by the SPE method for the determination of  $E_{\text{end}}$ . The spectra for non-zero ripple smaller than 1% follow the line for zero ripple (0%, = fit) and are not shown. The spectrum for zero ripple and no CCT+GEB is presented for comparison and to show  $E_{\text{end}}$ . All spectra were normalized to the same area.

### 3.4 Comparison of quantities

The comparison of kVp, PPV, and SPV for selected radiation qualities modeled by Monte Carlo simulations using a tube voltage of 60 kV and 120 kV is presented in table 5. The same voltage ripples were assumed as in section 3.3, and the distribution of voltages within the ripple range was uniform. The goal was to evaluate the differences between the quantities. The SPV agreed with the PPV value within 0.03% for the spectra generated with a voltage ripple of 4% or less. This difference was well below the SPV uncertainty of 0.23% for the 60 kV and 0.15% for the 120 kV ( $k = 1$ ) radiation qualities.

**Table 5.** kVp, PPV, and SPV for radiation qualities calculated by the Monte Carlo method for a nominal tube voltage of 60 kV and 120 kV and various voltage ripples with the uniform distribution of voltages within the ripple range. <sup>(1)</sup> The minimum and the maximum voltage is  $U_0 \pm \frac{1}{2}$ ·ripple. <sup>(2)</sup> The combined uncertainty. <sup>(3)</sup> Cannot be determined with the calculated detector spectrum assuming zero voltage ripple.

Nominal voltage, $U_0$ : 60 kV						
Ripple <sup>(1)</sup>	0%	0.6%	2%	4%	10%	$u^{(2)} (k = 1)$
kVp (kV)	60.000	60.180	60.600	61.200	63.000	0
PPV (kV)	60.000	60.000	60.005	60.018	60.113	0
SPV (kV)	60.00	60.00	60.00	60.00	— <sup>(3)</sup>	0.14
SPV/kVp −1	0%	−0.30%	−0.99%	−1.96%	−4.76%	0.23%
SPV/PPV −1	0%	0%	−0.01%	−0.03%	−0.19%	0.23%
Nominal voltage, $U_0$ : 120 kV						
kVp (kV)	120.000	120.360	121.200	122.400	126.000	0
PPV (kV)	120.000	120.000	120.005	120.022	120.137	0
SPV (kV)	120.00	120.00	120.00	120.00	— <sup>(3)</sup>	0.18
SPV/kVp −1	0.00%	−0.30%	−0.99%	−1.96%	−4.76%	0.15%
SPV/PPV −1	0%	0%	0%	−0.02%	−0.11%	0.15%

The maximum voltage ripple according to the manufacturer data sheet (see section 2.4) was about 1.2% (at 20 kV and 40 mA) for the 160 kV CMI high-voltage generator used in the range of the PPV definition (20–150 kV). At the voltages equal to or higher than 60 kV, the maximum ripple was less than 0.4% (at 40 mA). These findings lead to the conclusion that the 160 kV high-voltage generator available at CMI provides voltage of sufficient stability to allow the generation of X-ray fluence spectra whose properties are such that there is, within the derived uncertainty, no significant difference between the SPV obtained with the SPE method and the PPV. This is valid for any X-ray generator with a similar ripple, i.e., any modern high-frequency generator. Such generators are commonly used in calibration laboratories [35]. The SPV is not directly related to the PPV, given that the PPV is obtained from the knowledge of the time dependency of the tube voltage while the SPV evaluates one measured sample of a photon spectrum averaged over the detector acquisition time without any a priori knowledge of the given generator waveform. However, both quantities aim to deliver a value describing the real tube voltage approximated by an ideal tube voltage obtained with a constant tube potential.

On the other hand, the kVp values differed from the SPV values by half of the ripple. That is why this quantity is not derived with the SPE method unless the ripple is so low that it can be neglected or the deviation is included in the kVp combined uncertainty.

In the light of the presented results and the current state-of-the-art, it is meaningful to start a discussion about re-introducing in-beam X-ray spectrometry, or any other relevant method, as an alternative to voltage dividers to be allowed by the relevant standards for the determination of tube voltage, particularly if it is shown that the voltage ripple has an insignificant influence on the result. A standard represents a recommendation for the best possible practice. The current practice is to use high-frequency X-ray generators with very low voltage ripples. As was shown here, for such generators X-ray spectrometry can deliver a tube voltage value that agrees with the PPV within the uncertainty, thus effectively satisfying the requirements pertaining to the uncertainty of the PPV value. Current commercial compact spectrometers have made the in-beam measurement of X-ray spectra across the entire relevant range of energies (up to at least 300 keV) widely accessible. Many calibration laboratories today are already familiar with X-ray spectrometry, or they are working on its implementation. For laboratories that do not possess a voltage divider, the presented method is potentially a suitable alternative for determining the tube voltage. All such considerations indicate that the requirements placed by standards on the measurement of tube voltage may now be obsolete and that future revisions should reflect the capabilities currently available.

### 3.5 Influence of the tube current

The detector spectra acquired at CMI at the nominal tube voltages of 60 kV, 150 kV, and 200 kV across the whole available range of tube currents were used to estimate the variation of  $E_{\text{end}}$  with respect to the tube current. The high-energy part of each measured spectrum was fitted with the simulated spectrum with CCT+GEB applied. Examples of results for 60 kV and 200 kV tube voltages are presented in figure 18.  $E_{\text{end}}$  as a function of the tube current is plotted in figure 19.  $E_{\text{end}}$  varied within 0.5 keV over the entire range of available tube currents. The results indicated that  $E_{\text{end}}$  was stable within 0.1 keV up to roughly 12 mA and then increased before becoming stable again at high tube currents. In addition, the measurement with the 320 kV generator at the lowest tested current of 0.6 mA resulted in an increased  $E_{\text{end}}$ .

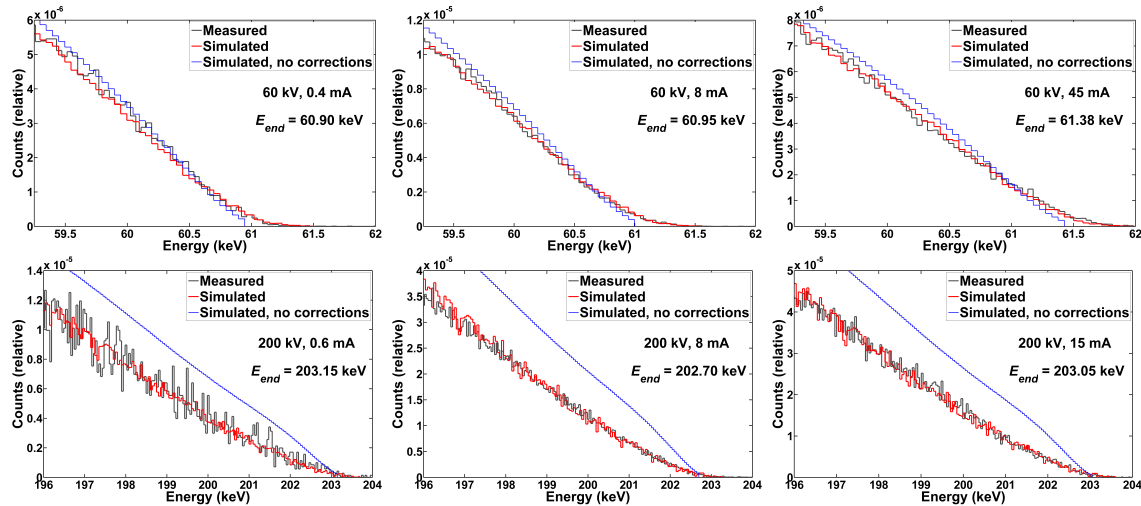


**Figure 18.** High-energy part of the measured 60 kV (nominal value; 160 kV generator; top row) and 200 kV (nominal value; 320 kV generator; bottom row) X-ray spectra at CMI fitted with the Monte Carlo calculated spectra with CCT+GEB applied, for different tube currents. The simulated smoothed spectra without CCT+GEB are shown for comparison and also visualize  $E_{\text{end}}$ .

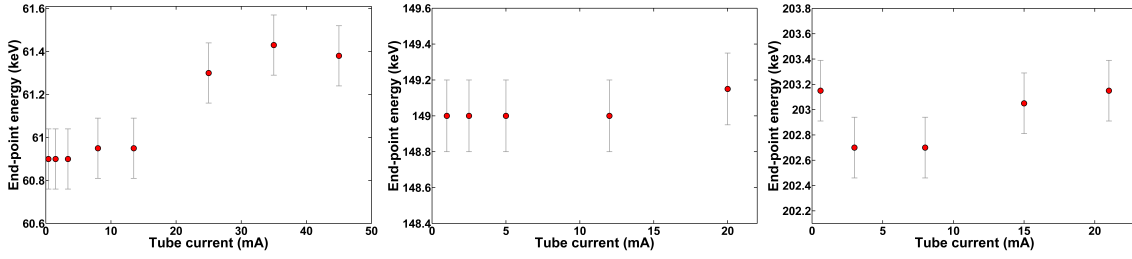


**Figure 19.** Relation between the tube current and the end-point energy for the nominal 60 kV (left), 150 kV (center), and 200 kV (right) tube voltages at CMI.

Clearly, the change of  $E_{\text{end}}$  relative to the tube current is typically small for both X-ray generators at CMI. It is therefore recommended to check  $E_{\text{end}}$  at various tube currents and then use the measured value only in the interval of tube currents where it remains stable. This can be achieved by the measurement of  $E_{\text{end}}$  at various distances or, if this is not possible, by changing the beam filtration. Also, information on the tube current should accompany the stated value of the measured  $E_{\text{end}}$ .

## 4 Conclusions

A detector with a small semiconductor sensing element and a suitable shielding and collimation system is a powerful tool for in-beam X-ray spectrometry. Precise characterization of the cadmium telluride X-123CdTe detector presented in this study and the previous publications ([1–3]) involving the energy calibration, energy resolution, description of the charge carrier transport, and Monte Carlo modelling, was originally performed with the aim of accurately measuring the X-ray beam energy distribution of photon fluence. The achievements gained have, however, also created the tools that enable the proposal of a method for determining the X-ray tube voltage using spectrometry.

The spectrometric practical end-point (SPE) method is based on the fit of the high-energy part of the measured detector spectrum with the detector spectrum obtained from Monte Carlo calculation. The method was demonstrated on narrow (N-series) radiation qualities as these are well suited to the method and the qualities are available in calibration laboratories. The method is, however, not restricted to these qualities. Corrections to the effects of the charge transport and collection occurring in the CdTe sensor were applied to the simulated spectra. The end-point energy of the measured spectrum was then obtained from the known energy of electrons hitting the anode used in the MC calculation and the energy offset of the simulated detector spectrum required to overlay the measured spectrum. The method does not use unfolding. However, a laboratory that has established in-beam X-ray spectrometry should already possess the tools required by the presented method. The accuracy of the energy calibration is crucial for the SPE method.

A clear relationship between the energy of an accelerated electron and the electric potential difference between X-ray tube electrodes enabled the definition of a quantity called the spectrometric practical voltage, SPV, which was determined by the presented SPE method. The SPV was compared to voltage divider readings taken at PTB. The relative and absolute differences between these readings and the SPV varied from 0.1% to 0.8% and from 0.15 keV to 1.16 keV, respectively, in the 20 to 300 kV tube voltage range. The combined uncertainty of the SPV varied between 0.13 and 0.33 keV for the radiation qualities realized with a tube voltage of 10 to 300 kV.

The influence of the tube current and the voltage ripple of the 160 kV and 320 kV generators installed at CMI were also investigated. An increase of up to 0.5 keV in the end-point energy of the spectra generated at the high tube current was measured compared to the spectra acquired at the low tube current. For this reason, the tube current should always be stated, and the SPV values are valid for the given current or interval of currents verified by measurement. It was observed that the influence of the voltage ripple on the measured detector spectra was insignificant. The ripple of high-voltage generators at CMI is always less than 1.2%, but typically less than 0.4%, and has a minimal impact on the shape of the end part of the detector spectrum. It was demonstrated that spectra realized with a ripple of up to about 2% result in the same SPV. Such characteristics translate to agreement between the SPV and the practical peak voltage, PPV, within 0.03%, which is below the uncertainty of the SPV.

For comparison, the end-point energy was also calculated with a commonly used simple linear fit of the straight high-energy part of the detector spectra. It was shown that the value obtained with the SPE method differed by  $-0.2$  to  $+1.5$  keV in the range of 10–300 kV. Up to 100 kV, both methods agreed within 0.2 keV.

Investigations of the energy calibration, the charge carrier transport, and the detector energy resolution were exploited to analyze the influence of their improper or neglected usage on the main characteristics of unfolded X-ray fluence spectra. The aim was to provide an overview of systematic errors on the half-value layer, selected conversion coefficients from air kerma to operational dosimetric quantities, and other parameters obtainable from the fluence spectra.

The current availability of commercial high-voltage generators with small voltage ripple and commercial compact X-ray spectrometers with integrated electrical cooling offers a new option for determining a quantity equivalent to the tube potential (or PPV), such as the proposed SPV, using X-ray spectrometry with low uncertainty. It seems meaningful to start a discussion about re-introducing in-beam X-ray spectrometry as an alternative to voltage dividers in future revisions of the relevant standards that define reference radiation conditions.

Continuous improvements in the in-beam X-ray spectrometry methods utilizing the compact X-123CdTe detector have greatly extended CMI's capabilities for characterizing those X-ray qualities realized at CMI. The easy transportability of the measurement setup allows spectrometric characterization of X-ray radiation qualities to be performed at other sites as well.

## Acknowledgments

The measurements performed at PTB were funded by the project 22NRM01 TraMeXI, which has received funding from the European Partnership on Metrology, co-financed from the European Union's Horizon Europe Research and Innovation Programme and by the Participating States. The authors would like to thank Reinulf Böttcher for the technical support provided during the measurement campaign at PTB. This work was also partly funded by an Institutional Subsidy for Long-Term Conceptual Development of a Research Organization granted to the Czech Metrology Institute by the Ministry of Industry and Trade of the Czech Republic.

## 5 Abbreviations

**AAPM** American Association of Physicists in Medicine

**CCT** charge carrier transport

<b>CdTe</b>	cadmium telluride
<b>CMI</b>	Czech Metrology Institute
<b>CZT</b>	cadmium zinc telluride
<b>DDEP</b>	Decay Data Evaluation Project
<b><math>E_{\text{end}}</math></b>	end-point energy of X-ray spectrum
<b><math>E_0</math></b>	energy of monoenergetic primary electrons
<b>EPICS</b>	Electron Photon Interaction Cross Sections
<b>FE</b>	full energy
<b>FEP</b>	full-energy peak
<b>FWHM</b>	full width at half maximum
<b>GEB</b>	Gaussian energy broadening
<b>HPGe</b>	high-purity germanium
<b>HVL</b>	half-value layer
<b>IEC</b>	International Electrotechnical Commission
<b>ISO</b>	International Organization for Standardization
<b>kVp</b>	peak kilovoltage
<b>MC</b>	Monte Carlo
<b>MCNP</b>	software for computer simulations of ionization radiation transport in matter
<b>PPV</b>	practical peak voltage
<b>PTB</b>	Physikalisch-Technische Bundesanstalt
<b>PTRAC</b>	particle track
<b>RD</b>	relative difference
<b>SPE</b>	spectrometric practical end-point
<b>SPV</b>	spectrometric practical voltage

## A Systematic errors caused by omission of detector effects

**Table 6.** Comparison of mean photon energy of X-ray spectra realized at CMI,  $\bar{E}(\Phi)$ , unfolded by various response matrices (RMs): 1. Reference RM (RM1; high-count-rate regime, CCT+GEB applied). 2. CCT neglected (RM2; high-count-rate regime, GEB applied). 3. CCT+GEB neglected (RM3; high-count-rate regime, CCT+GEB not applied). 4. As RM, but energy calibration for visualization was used (RM1a). 5. As RM, but energy calibration for low-count-rate regime was used (RM1b).  $RD_{RMx} = \bar{E}(\Phi)_{RMx} / \bar{E}(\Phi)_{RM1} - 1$ .

X-ray quality	$\bar{E}(\Phi)_{RM1}$ (keV)	$RD_{RM2}$	$RD_{RM3}$	$RD_{RM1a}$	$RD_{RM1b}$
<b>N-10</b>	8.07	−1.7%	−1.7%	0.2%	−0.3%
<b>N-15</b>	11.99	−1.3%	−1.4%	0.2%	−0.2%
<b>N-20</b>	16.00	−0.9%	−0.9%	0.2%	−0.2%
<b>N-25</b>	19.98	−0.6%	−0.6%	0.1%	−0.2%
<b>N-30</b>	24.24	−0.5%	−0.5%	0.1%	−0.2%
<b>N-40</b>	32.85	−0.6%	−0.6%	0.1%	−0.2%
<b>N-60</b>	47.73	−0.6%	−0.6%	0.1%	−0.2%
<b>N-80</b>	64.62	−0.7%	−0.7%	0.1%	−0.2%
<b>N-100</b>	82.83	−0.9%	−1.0%	0.1%	−0.2%
<b>N-120</b>	100.20	−1.1%	−1.1%	0.1%	−0.1%
<b>N-150</b>	118.20	−1.4%	−1.4%	0.1%	−0.2%
<b>N-200</b>	166.20	−1.4%	−1.4%	0.1%	−0.1%
<b>N-250</b>	208.70	−1.6%	−1.6%	0.0%	−0.1%
<b>N-300</b>	248.10	−2.3%	−2.3%	0.1%	−0.1%
<b>RQR2</b>	28.06	0.2%	−0.6%	0.1%	−0.2%
<b>RQR3</b>	32.32	0.0%	−0.6%	0.1%	−0.2%
<b>RQR4</b>	36.51	−0.1%	−0.6%	0.1%	−0.2%
<b>RQR5</b>	40.33	−0.1%	−0.6%	0.1%	−0.1%
<b>RQR6</b>	43.96	−0.2%	−0.6%	0.2%	0.0%
<b>RQR7</b>	47.66	−0.4%	−0.8%	0.0%	−0.2%
<b>RQR8</b>	50.79	−0.5%	−1.0%	0.1%	−0.1%
<b>RQR9</b>	56.44	−0.6%	−1.1%	0.1%	−0.2%
<b>RQR10</b>	63.89	−1.0%	−0.9%	0.1%	−0.1%
<b>TW10</b>	7.40	−1.5%	−1.5%	0.2%	−0.3%
<b>TW15</b>	9.97	0.1%	−2.0%	0.2%	−0.3%
<b>TW20</b>	12.53	0.2%	−1.5%	0.2%	−0.2%
<b>TW30</b>	19.49	0.3%	−0.9%	0.2%	−0.3%
<b>TW50</b>	29.22	0.0%	−0.6%	0.1%	−0.2%
<b>TW70</b>	41.90	−0.1%	−0.6%	0.1%	−0.1%
<b>TW100</b>	52.38	−0.5%	−1.0%	0.0%	−0.2%

**Table 7.** Comparison of 1<sup>st</sup> half-value layer (1<sup>st</sup> HVL) in Al or Cu of X-ray spectra realized at CMI, unfolded by various response matrices (RMs). See table 6 caption for RM definitions.  $RD_{RMx} = (1^{st} \text{ HVL})_{RMx} / (1^{st} \text{ HVL})_{RM1} - 1$ .

<b>X-ray quality</b>	<b>1<sup>st</sup> HVL (mm)</b>	<b><math>RD_{RM2}</math></b>	<b><math>RD_{RM3}</math></b>	<b><math>RD_{RM1a}</math></b>	<b><math>RD_{RM1b}</math></b>
<b>N-10</b>	0.048 Al	−8.1%	−8.5%	0.7%	−0.9%
<b>N-15</b>	0.148 Al	−6.1%	−7.7%	0.5%	−0.8%
<b>N-20</b>	0.338 Al	−4.8%	−5.2%	0.5%	−0.7%
<b>N-25</b>	0.646 Al	−3.1%	−3.3%	0.4%	−0.6%
<b>N-30</b>	1.130 Al	−2.4%	−2.4%	0.4%	−0.6%
<b>N-40</b>	2.574 Al	−2.1%	−2.1%	0.3%	−0.4%
<b>N-60</b>	0.234 Cu	−2.4%	−2.4%	0.4%	−0.5%
<b>N-80</b>	0.568 Cu	−2.2%	−2.1%	0.3%	−0.5%
<b>N-100</b>	1.087 Cu	−2.4%	−2.4%	0.3%	−0.4%
<b>N-120</b>	1.686 Cu	−2.5%	−2.3%	0.2%	−0.3%
<b>N-150</b>	2.348 Cu	−2.5%	−2.6%	0.2%	−0.3%
<b>N-200</b>	4.011 Cu	−1.8%	−1.8%	0.1%	−0.1%
<b>N-250</b>	5.176 Cu	−1.5%	−1.5%	0.1%	0.0%
<b>N-300</b>	6.033 Cu	−1.8%	−1.7%	0.1%	0.0%
<b>RQR2</b>	1.379 Al	−0.3%	−3.0%	0.4%	−0.6%
<b>RQR3</b>	1.755 Al	−0.7%	−2.8%	0.4%	−0.6%
<b>RQR4</b>	2.193 Al	−0.8%	−1.6%	0.4%	−0.5%
<b>RQR5</b>	2.612 Al	−0.9%	−2.7%	0.3%	−0.5%
<b>RQR6</b>	3.007 Al	−1.0%	−2.8%	0.4%	−0.4%
<b>RQR7</b>	3.550 Al	−1.0%	−2.9%	0.1%	−0.5%
<b>RQR8</b>	4.035 Al	−1.3%	−3.3%	0.3%	−0.4%
<b>RQR9</b>	5.059 Al	−2.0%	−4.3%	0.1%	−0.5%
<b>RQR10</b>	6.614 Al	−3.0%	−3.3%	0.4%	−0.3%
<b>TW10</b>	0.034 Al	−6.1%	−6.3%	0.7%	−0.9%
<b>TW15</b>	0.071 Al	−4.2%	−11.3%	0.6%	−0.9%
<b>TW20</b>	0.115 Al	−2.0%	−8.4%	0.7%	−0.8%
<b>TW30</b>	0.389 Al	−2.1%	−7.5%	0.2%	−0.9%
<b>TW50</b>	1.064 Al	−1.5%	−4.5%	0.6%	−0.5%
<b>TW70</b>	3.106 Al	−0.9%	−2.5%	0.3%	−0.5%
<b>TW100</b>	4.659 Al	−1.4%	−3.1%	0.1%	−0.5%

**Table 8.** Comparison of homogeneity coefficient,  $h$ , for Al or Cu of X-ray spectra realized at CMI, unfolded by various response matrices (RMs). See table 6 caption for RM definitions.  $RD_{RMx} = h_{RMx}/h_{RM1} - 1$ .

X-ray quality	$h$ (material)	$RD_{RM2}$	$RD_{RM3}$	$RD_{RM1a}$	$RD_{RM1b}$
<b>N-10</b>	0.934 (Al)	−3.0%	−3.2%	0.0%	0.0%
<b>N-15</b>	0.918 (Al)	−2.1%	−3.6%	0.0%	0.0%
<b>N-20</b>	0.901 (Al)	−2.0%	−2.4%	0.1%	0.1%
<b>N-25</b>	0.907 (Al)	−1.2%	−1.5%	0.0%	0.0%
<b>N-30</b>	0.917 (Al)	−0.8%	−0.9%	0.0%	0.0%
<b>N-40</b>	0.936 (Al)	−0.6%	−0.6%	0.0%	0.0%
<b>N-60</b>	0.899 (Cu)	−0.7%	−0.8%	0.0%	0.1%
<b>N-80</b>	0.934 (Cu)	−0.5%	−0.6%	0.0%	−0.1%
<b>N-100</b>	0.949 (Cu)	−0.4%	−0.4%	0.0%	0.1%
<b>N-120</b>	0.965 (Cu)	−0.6%	−0.6%	−0.1%	0.0%
<b>N-150</b>	0.956 (Cu)	−0.4%	−0.5%	0.0%	0.0%
<b>N-200</b>	0.985 (Cu)	−0.3%	−0.3%	0.1%	0.0%
<b>N-250</b>	0.991 (Cu)	−0.3%	−0.3%	0.1%	0.1%
<b>N-300</b>	0.994 (Cu)	−0.3%	−0.3%	0.1%	0.1%
<b>RQR2</b>	0.810 (Al)	−0.8%	−1.3%	0.1%	−0.1%
<b>RQR3</b>	0.758 (Al)	−0.7%	−1.3%	0.1%	−0.1%
<b>RQR4</b>	0.731 (Al)	−0.4%	−2.1%	0.2%	0.0%
<b>RQR5</b>	0.710 (Al)	−0.6%	−1.1%	−0.1%	−0.3%
<b>RQR6</b>	0.687 (Al)	−0.5%	−0.9%	0.1%	−0.1%
<b>RQR7</b>	0.681 (Al)	−0.3%	−0.8%	0.2%	−0.1%
<b>RQR8</b>	0.677 (Al)	−0.2%	−0.8%	0.1%	0.0%
<b>RQR9</b>	0.685 (Al)	−0.6%	−1.3%	0.0%	−0.2%
<b>RQR10</b>	0.719 (Al)	−1.1%	−1.4%	0.3%	−0.1%
<b>TW10</b>	0.881 (Al)	−1.0%	−1.2%	0.0%	0.0%
<b>TW15</b>	0.820 (Al)	−4.4%	−5.1%	0.0%	0.0%
<b>TW20</b>	0.763 (Al)	−2.3%	−3.0%	0.1%	0.0%
<b>TW30</b>	0.672 (Al)	−2.3%	−3.9%	−0.1%	0.0%
<b>TW50</b>	0.667 (Al)	−1.7%	−2.4%	0.1%	0.0%
<b>TW70</b>	0.746 (Al)	−0.5%	−0.9%	0.0%	−0.2%
<b>TW100</b>	0.716 (Al)	−0.4%	−0.7%	0.1%	0.0%

**Table 9.** Comparison of conversion coefficient from air kerma to personal dose equivalent  $H_p(10; 0^\circ)$  in ICRU slab phantom at an angle of radiation incidence of  $0^\circ$ ,  $h_{pK}(10; 0^\circ)_{\text{slab}}$ , of selected X-ray radiation qualities realized at CMI unfolded by various response matrices (RMs). See table 6 caption for RM definitions. Data for RQR and TW qualities are given for completeness only as these qualities are not used for testing in radiological protection.  $RD_{\text{RMx}} = h_{pK}(10; 0^\circ)_{\text{slab, RMx}}/h_{pK}(10; 0^\circ)_{\text{slab, RM1}} - 1$ .

X-ray quality	$h_{pK}(10; 0^\circ)_{\text{slab}}$	$RD_{\text{RM2}}$	$RD_{\text{RM3}}$	$RD_{\text{RM1a}}$	$RD_{\text{RM1b}}$
<b>N-10</b>	4.02E-04	−16.8%	−17.6%	4.5%	−5.9%
<b>N-15</b>	0.072	−9.0%	−10.0%	1.3%	−1.8%
<b>N-20</b>	0.305	−4.6%	−4.9%	0.6%	−0.8%
<b>N-25</b>	0.561	−2.1%	−2.3%	0.3%	−0.5%
<b>N-30</b>	0.800	−1.2%	−1.3%	0.2%	−0.3%
<b>N-40</b>	1.189	−0.9%	−0.9%	0.1%	−0.3%
<b>N-60</b>	1.664	−0.6%	−0.7%	0.1%	−0.1%
<b>N-80</b>	1.893	−0.2%	−0.2%	0.0%	−0.1%
<b>N-100</b>	1.882	0.1%	0.1%	0.0%	0.0%
<b>N-120</b>	1.806	0.3%	0.3%	−0.1%	0.1%
<b>N-150</b>	1.722	0.3%	0.3%	0.0%	0.1%
<b>N-200</b>	1.561	0.4%	0.4%	0.0%	0.1%
<b>N-250</b>	1.473	0.3%	0.3%	−0.1%	0.0%
<b>N-300</b>	1.417	0.5%	0.5%	0.0%	0.0%
<b>RQR2</b>	0.906	−0.2%	−1.5%	0.2%	−0.3%
<b>RQR3</b>	1.033	−0.4%	−1.4%	0.2%	−0.3%
<b>RQR4</b>	1.151	−0.3%	−1.3%	0.2%	−0.2%
<b>RQR5</b>	1.245	−0.4%	−1.1%	0.2%	−0.2%
<b>RQR6</b>	1.319	−0.4%	−1.1%	0.2%	−0.1%
<b>RQR7</b>	1.399	−0.4%	−1.1%	0.0%	−0.1%
<b>RQR8</b>	1.457	−0.5%	−1.2%	0.1%	−0.1%
<b>RQR9</b>	1.549	−0.6%	−1.3%	0.0%	−0.1%
<b>RQR10</b>	1.636	−0.7%	−0.9%	0.1%	−0.1%
<b>TW10</b>	1.59E-04	−10.4%	−10.5%	4.5%	−6.1%
<b>TW15</b>	0.018	2.8%	−13.3%	1.7%	−2.3%
<b>TW20</b>	0.081	0.1%	−8.6%	0.9%	−1.3%
<b>TW30</b>	0.405	−1.0%	−5.0%	0.2%	−0.7%
<b>TW50</b>	0.817	−0.8%	−2.4%	0.3%	−0.3%
<b>TW70</b>	1.328	−0.4%	−1.0%	0.1%	−0.1%
<b>TW100</b>	1.526	−0.5%	−1.0%	0.0%	−0.2%

**Table 10.** Comparison of conversion coefficient from air kerma to the directional dose equivalent  $H'(0.07)$  at an angle of radiation incidence of  $0^\circ$ ,  $h'_K(0.07; 0^\circ)$ , of selected X-ray radiation qualities realized at CMI unfolded by various response matrices (RMs). See table 6 caption for RM definitions. Data for RQR and TW qualities are given for completeness only as these qualities are not used for testing in radiological protection.  $RD_{RMx} = h'_K(0.07; 0^\circ)_{RMx} / h'_K(0.07; 0^\circ)_{RM1} - 1$ .

X-ray quality	$h'_K(0.07; 0^\circ)$	$RD_{RM2}$	$RD_{RM3}$	$RD_{RM1a}$	$RD_{RM1b}$
<b>N-10</b>	0.874	0.9%	1.6%	0.1%	-0.1%
<b>N-15</b>	0.963	-0.4%	-0.5%	0.0%	0.0%
<b>N-20</b>	0.997	-0.2%	-0.2%	0.0%	0.0%
<b>N-25</b>	1.043	-0.2%	-0.3%	0.0%	-0.1%
<b>N-30</b>	1.107	-0.2%	-0.2%	0.1%	-0.1%
<b>N-40</b>	1.261	-0.3%	-0.4%	0.1%	-0.1%
<b>N-60</b>	1.484	-0.3%	-0.3%	0.1%	-0.1%
<b>N-80</b>	1.594	-0.1%	-0.1%	0.0%	-0.1%
<b>N-100</b>	1.596	0.1%	0.1%	-0.1%	0.0%
<b>N-120</b>	1.550	0.2%	0.2%	0.0%	0.0%
<b>N-150</b>	1.500	0.3%	0.3%	-0.1%	0.0%
<b>N-200</b>	1.386	0.3%	0.3%	0.0%	0.1%
<b>N-250</b>	1.332	0.2%	0.2%	0.0%	0.0%
<b>N-300</b>	1.312	0.2%	0.2%	0.0%	0.0%
<b>RQR2</b>	1.151	0.0%	-0.3%	0.1%	-0.1%
<b>RQR3</b>	1.204	-0.1%	-0.4%	0.1%	-0.1%
<b>RQR4</b>	1.255	-0.2%	-0.5%	0.0%	-0.2%
<b>RQR5</b>	1.296	-0.2%	-0.5%	0.0%	-0.1%
<b>RQR6</b>	1.329	-0.2%	-0.5%	0.1%	-0.1%
<b>RQR7</b>	1.365	-0.1%	-0.4%	0.0%	-0.1%
<b>RQR8</b>	1.392	-0.2%	-0.5%	0.0%	-0.1%
<b>RQR9</b>	1.434	-0.3%	-0.6%	0.1%	-0.1%
<b>RQR10</b>	1.472	-0.4%	-0.5%	0.0%	-0.1%
<b>TW10</b>	0.889	3.3%	4.8%	0.0%	0.0%
<b>TW15</b>	0.915	1.7%	-0.7%	0.1%	-0.1%
<b>TW20</b>	0.946	-0.2%	-0.7%	0.0%	-0.1%
<b>TW30</b>	1.019	-0.1%	-0.5%	0.0%	-0.1%
<b>TW50</b>	1.134	-0.1%	-0.4%	0.1%	-0.1%
<b>TW70</b>	1.331	-0.1%	-0.4%	0.1%	-0.1%
<b>TW100</b>	1.422	-0.2%	-0.5%	0.0%	-0.1%

## References

- [1] J. Šolc et al., *Practical X-ray beam spectrometry with cadmium telluride detector in 10–300 kVp range at Czech Metrology Institute. Part I. Instrumentation*, [2022 JINST 17 P10002](#).
- [2] J. Šolc, J. Šmoldasová, L. Štemberková, V. Sochor and Z. Vykydal, *Improved setup and characterization of cadmium telluride detector for in-beam X-ray spectrometry up to 300 kV at Czech Metrology Institute*, [JINST P.1 \(add -1\)](#)
- [3] J. Šolc et al., *Practical X-ray beam spectrometry with cadmium telluride detector in 10–300 kVp range at Czech Metrology Institute. Part II. Unfolding*, [2022 JINST 17 P10003](#).
- [4] IEC 61676:2023, *Medical electrical equipment - Dosimetric instruments used for non-invasive measurement of X-ray tube voltage in diagnostic radiology*, International Electrotechnical Commission (2023).
- [5] IEC 61267:2005, *Medical diagnostic X-ray equipment — Radiation conditions for use in the determination of characteristics*, International Electrotechnical Commission (2005).
- [6] A.B. Wolbarst, *Physics of Radiology*, Medical Physics Publishing, U.K. (2005).
- [7] M. Krmar, N. Bucalović, M. Baucal and N. Jovančević, *Possible use of CdTe detectors in kVp monitoring of diagnostic X-ray tubes*, [Nucl. Instrum. Meth. A 622 \(2010\) 256](#).
- [8] M.C. Silva et al., *Determination of the voltage applied to x-ray tubes from the bremsstrahlung spectrum obtained with a silicon PIN photodiode*, [Med. Phys. 27 \(2000\) 2617](#).
- [9] R.A. Terini et al., *Comprehensive analysis of the spectrometric determination of voltage applied to X-ray tubes in the radiography and mammography energy ranges using a silicon PIN photodiode*, [Br. J. Radiol. 77 \(2004\) 395](#).
- [10] J. Law, K. Faulkner and S. Smith, *Measurement of X-ray tube potential in the mammographic region*, [Phys. Med. Biol. 34 \(1989\) 717](#).
- [11] S.J. Shepherd et al., *Quality Control in Diagnostic Radiology*, AAPM Report 74 American Association of Physicists in Medicine, Alexandria, VA, U.S.A. (2002) [[DOI: 10.37206/73](#)].
- [12] A.F. Jacobson, J.R. Cameron, M.P. Siedband and J. Wagner, *Test cassette for measuring peak tube potential of diagnostic x-ray machines*, [Med. Phys. 3 \(1976\) 19](#).
- [13] J.C. Giarratano, R.G. Waggener, J.M. Hevezi and R.J. Shalek, *Comparison of voltage-divider, modified Ardran-Crooks cassette, and Ge(Li) spectrometer methods to determine the peak kilovoltage (kVp) of diagnostic x-ray units*, [Med. Phys. 3 \(1976\) 142](#).
- [14] L.C. Mihailescu, *X-ray spectrometry with germanium detector at a dosimetry calibration laboratory*, [2023 JINST 18 P09037](#).
- [15] W. de Vries, *Spectrometric methods used in the calibration of radiodiagnostic measuring instruments*, in the proceedings of the *11th Annual Symposium of the Belgian Hospital Physicists Association*, Gent, Belgium, December 8–9 (1995), pp. 217–221.
- [16] ISO 4037-1:1996, *X and gamma reference radiation for calibrating dosimeters and doserate meters and for determining their response as a function of photon energy. Part 1: Radiation characteristics and production methods*, International Organization for Standardization (1996).
- [17] *X-123CdTe Complete X-Ray & Gamma Ray Spectrometer*, AMPTEK, Inc., U.S.A., <https://www.amptek.com/internal-products/x-123-cdte-complete-x-ray-gamma-ray-spectrometer-with-cdte-detector>.
- [18] *DPPMCA Display & Acquisition Software*, AMPTEK, Inc., U.S.A., <https://www.amptek.com/software/dp5-digital-pulse-processor-software/dppmca-display-acquisition-software>.

- [19] *colorFabb SteelFill 750 g filament*, <https://colorfabb.com/steelfill>.
- [20] *Prusament PETG Tungsten 75% 1 kg filament*, <https://www.prusa3d.com/product/prusament-petg-tungsten-75-1kg>.
- [21] ISO 4037-1:2019(E), *Radiological protection — X and gamma reference radiation for calibrating doseimeters and doserate meters and for determining their response as a function of photon energy — Part 1: Radiation characteristics and production methods*, Second edition, International Organization for Standardization (2019).
- [22] DIN 6809-4:2020-04, *Clinical dosimetry — Part 4: X-ray therapy with X-ray tube voltages between 10 kV and 300 kV*, Deutsche Institut für Normung e.V. (2020).
- [23] H.M. Kramer, H.J. Selbach and W.J. Iles, *The practical peak voltage of diagnostic X-ray generators*, *Br. J. Radiol.* **71** (1998) 200.
- [24] *DDEP, Decay Data Evaluation Project*, <http://www.lnhb.fr/donnees-nucleaires/donnees-nucleaires-tableau/>.
- [25] J.Ch. Werner, *MCNP<sup>®</sup> User's Manual, Code Version 6.2*, LA-UR-17-29981, Los Alamos National Laboratory, Los Alamos, NM, U.S.A. (2017).
- [26] MCNP<sup>®</sup> code website, <https://mcnp.lanl.gov/>.
- [27] K.J. Adams, *Electron Upgrade for MCNP4B*, X-5-RN(U)-00-14, Los Alamos National Laboratory, Los Alamos, NM, U.S.A. (2000).
- [28] J.Ch. Werner et al., *MCNP Version 6.2 Release Notes*, LA-UR-18-20808, Los Alamos National Laboratory, Los Alamos, NM, U.S.A. (2018).
- [29] D.E. Cullen, *EPICS2014: Electron Photon Interaction Cross Sections (Version 2014)*, IAEA-NDS-218, International Atomic Energy Agency, Vienna, Austria (2014).
- [30] R. Bujila, A. Omar and G. Poludniowski, *A validation of SpekPy: A software toolkit for modelling X-ray tube spectra*, *Phys. Med.* **75** (2020) 44.
- [31] SpekPy software website, [https://bitbucket.org/spekpy/spekpy\\_release/wiki/Home](https://bitbucket.org/spekpy/spekpy_release/wiki/Home).
- [32] G. Poludniowski, A. Omar, R. Bujila and P. Andreo, *Technical Note: SpekPy v2.0 — a software toolkit for modeling x-ray tube spectra*, *Med. Phys.* **48** (2021) 3630.
- [33] L. Rinaldi et al. *Implementation of the ISO 4037:2019 norm using voltage dividers and X-ray spectrometry*, submitted to *Radiat. Prot. Dosimetry*, (2024).
- [34] ISO 4037-3:2019(E), *Radiological protection — X and gamma reference radiation for calibrating doseimeters and doserate meters and for determining their response as a function of photon energy — Part 3: Calibration of area and personal doseimeters and the measurement of their response as a function of energy and angle incidence*, Second edition, International Organization for Standardization (2019).
- [35] IAEA, *Implementation of the International Code of Practice on Dosimetry in Diagnostic Radiology (TRS 457): Review of Test Results*, IAEA Human Health Reports No. 4, International Atomic Energy Agency, Vienna, Austria (2011).